RADIAL DISTRIBUTION FUNCTION IN THE BRUECKNER THEORY OF INTERACTING FERMION SYSTEMS*

By J. Dąbrowski and H. S. Köhler

Institute of Nuclear Research, Warsaw**
and
Department of Physics, University of Arizona***

(Received September 28, 1981)

Perturbation theory of the radial distribution function is described by Goldstone diagrams. Our selection of diagrams is guided by Brueckner theory. Thus two-hole line particle–particle ladder diagrams are selected with kinetic energy propagators in a low density approximation. In another selection of diagrams the hole lines are dressed by bubble-insertions in a low-order Brueckner approximation. The normalization of the radial distribution function is discussed. Calculations are presented for nuclear matter with several simplified interactions and for liquid-^{3}He with the Lennard-Jones 6–12 potential.

PACS numbers: 21.65.+f, 67.50.–b

1. Introduction

We shall in this paper be concerned with ground state properties of an infinite system of fermions. We are in particular interested in calculating the radial distribution function assuming that the interaction between the fermions is given by a local two-body force.

A complete description of a quantum system is given by the total wave function. The density-matrix provides an alternative description in coordinate space. One is often not interested in all the information provided by this matrix. The reduced n-body density-matrix is obtained from the full density-matrix of the N particles by integrating over all coordinates but n. In order to calculate the energy of a system of particles interacting via two-body forces it is for example sufficient to know only the one- and the two-body density-matrix to compute the kinetic and the potential energy respectively. If the two-body forces are local the problem is simplified further. The calculation of the potential energy

* Supported by the Polish-U.S. Maria Skłodowska-Curie Fund under Grant P-F7F037P, and in part by NSF Grant PHY-790264.

** Address: Instytut Badań Jądrowych, Hoża 69, 00-681 Warszawa, Poland.
*** Address: Department of Physics, University of Arizona, Tucson, Arizona 85721, USA.

then requires only the diagonal part of the density-matrix, i.e., only the two-body density. This density is directly related to the radial distribution function defined in Section 2. It plays an important part in the theory of many body systems [1]. It is usually obtained in the course of calculating the energy by the cluster expansion method with Jastrow correlations [2].

A viable alternative to these methods of calculating the ground-state energy is Brueckner's method. It involves a perturbative expansion in which selected terms (diagrams) are summed. This method has been applied to the calculation of saturation and binding of fermion systems. Together with the e^S-method it is sometimes referred to as a coupled--cluster expansion. Brueckner theory applied to the calculation of the energy customarily involves an expansion in terms of the interacting part of the Hamiltonian. The zero-order energy is the kinetic energy of the non-interacting fermion system.

In this paper we apply these rules to the calculation of the radial distribution function, the expectation value of a two-body operator. Once this function is known the potential energy of the system is easily calculated. The rules are also applied to the calculation of the kinetic energy; this being the expectation value of a one-body operator. It is to be noted that in the infinite system with which we deal, the momentum is a good quantum number, and the kinetic energy operator is diagonal in momentum space, as is the one body density--matrix.

There are thus two separate ways to calculate perturbatively the total energy. The first is the customary Brueckner expansion of the total energy. The second is the calculation of the potential energy from the radial distribution function together with a calculation of the kinetic energy. If the same type of diagrams are included in the two separate calculations the answers should agree. The second method, the one we are introducing in this paper gives however more information in at least two respects. Firstly, it gives separately the potential and the kinetic energy of the system. Secondly, it gives the radial distribution function. This is the real motivation for this work as this function contains important information that complements say the traditional Brueckner calculation of the energy (which is only one number). To give an example: In order to improve the accuracy of the energy-calculation more diagrams are added, e.g., as in Day's nuclear matter calculations including three-hole line diagrams [3, 4]. It would be of value to know how these improvements affect the distribution-function. Are the corrections short- or long-ranged? Another example: An approximate treatment, e.g., by some insertions in particle-lines, can give the same total energy as a more correct treatment. But are the radial distribution functions the same or significantly different in the two cases?

The latter example can in the case in liquid-^{3}He be resolved experimetally as the radial distribution function is already measured in this case. Hopefully it will also be known for nuclear matter from (e,e′) scattering [5]. In view of this, the calculation of the radial distribution function by perturbation methods is of value. It would also be a complement to the Jastrow approach in which this function is obtained as a consequence of the method itself. In the past few years this approach has reached a high degree of sophistication. A comparison of the two methods (Brueckner and Jastrow) would be much more informative if not only the energies but also the radial distribution functions calculated by each

of the methods could be compared. In addition we propose to calculate the state-dependence of the correlations, not readily done in Jastrow-work.

In our discussion above two-body forces only were implied. Three-body forces would involve the three-body density etc.. It may very well be that in atomic nuclei the mesonic degrees of freedom are more important than hitherto believed so that many-body forces are indeed not negligible. One avenue of approach to study this problem would be the theoretical and experimental determination of the two-body density.

Our paper is organised as follows. In Section 2 the radial distribution function is defined in terms of the N-body wave function as an expectation value of a two-body operator. In Section 3 the perturbation expansion of this two-body operator is shown in terms of Goldstone diagrams. Most of our subsequent discussions and results are based on these diagrams to various orders and their rules. Section 4 gives the result of a low--density approximation. Section 5 discusses the important aspect of the normalisation of the radial distribution function in this approximation. In Sections 6 and 7 the expressions for the expectation value of the potential and the kinetic energy respectively are shown. In Section 8 and in Appendices A and B we show some details of methods used in the calculations, the results of which are presented in Section 9. The results shown are for nuclear matter with some different interactions and for liquid-^{3}He with the Lennard–Jones 6–12 potential. For most systems it is necessary to go beyond the low-density approximation of Section 4. In Section 10 we discuss a three-hole line expansion, which is analogous to the so-called low-order Brueckner approximation. However, some difficulties are encountered here as described in part D of this Section. Section 11, finally, summarizes the results of our investigation and contains some concluding remarks.

2. *Definition of the radial distribution function*

We consider the ground state of a homogeneous N fermion system described by the wave function

$$\Psi = \Psi(\boldsymbol{r}_1\xi_1, \ldots, \boldsymbol{r}_i\xi_i, \ldots, \boldsymbol{r}_N\xi_N), \tag{2.1}$$

where $\boldsymbol{r}_i$ is the space coordinate and ξ_i the spin-isospin coordinate of the i-th particle. The density of the system $\varrho = N/\Omega$ (Ω = volume of the periodicity box) is connected with the Fermi momentum k_F (we measure all momenta in units of $\hbar$):

$$\varrho = \nu k_F^3/6\pi^2, \tag{2.2}$$

where ν is the spin-isospin degeneracy ($\nu = 4$ for nuclear matter, $\nu = 2$ for liquid ^{3}He).

The definition of the radial distribution function g is:

$$\varrho^2 g(\boldsymbol{r}_1, \boldsymbol{r}_2) = G(\boldsymbol{r}_1, \boldsymbol{r}_2) = N(N-1) \int d\xi_1 d\xi_2 d\boldsymbol{r}_3 d\xi_3 \ldots d\boldsymbol{r}_N d\xi_N |\Psi(\boldsymbol{r}_1\xi_1, \ldots, \boldsymbol{r}_N\xi_N)|^2/(\Psi|\Psi), \tag{2.3}$$

where $(\Psi|\Psi)$ is the normalization integral. The function G is the diagonal part of the two--body density matrix, i.e., the two-body density discussed in the introduction. For a homog-

eneous and isotropic system, g depends only on the distance r_{12},

$$g(\boldsymbol{r}_1, \boldsymbol{r}_2) = g(r_{12}). \tag{2.4}$$

Instead of (2.3) we may use an equivalent definition:

$$G(\boldsymbol{x}, \boldsymbol{y}) = (\Psi| \sum_{\substack{i=1 \\ i \neq j}}^{N} \sum_{j=1}^{N} \delta(\boldsymbol{r}_i - \boldsymbol{x}) \delta(\boldsymbol{r}_j - \boldsymbol{y}) |\Psi)/(\Psi|\Psi)$$

$$= N(N-1) (\Psi|\delta(\boldsymbol{r}_1 - \boldsymbol{x}) \delta(\boldsymbol{r}_2 - \boldsymbol{y}) |\Psi)/(\Psi|\Psi). \tag{2.5}$$

Let us compare (2.5) with the expression for the expectation value $\langle W \rangle$ of a two-body operator

$$W = \sum_{i<j} \sum w(r_{ij}), \tag{2.6}$$

$$\langle W \rangle = (\Psi| \sum_{i<j} \sum w(r_{ij}) |\Psi)/(\Psi|\Psi) = \tfrac{1}{2} N(N-1) (\Psi|w(r_{12}) |\Psi)/(\Psi|\Psi). \tag{2.7}$$

We see that $G(\boldsymbol{x}, \boldsymbol{y})$ is the expectation value of $\tilde{W}$,

$$\tilde{W} = \sum_{i<j} \sum \tilde{w}(r_{ij}), \quad \tilde{w}(r_{ij}) = 2\delta(\boldsymbol{r}_i - \boldsymbol{x}) \delta(\boldsymbol{r}_j - \boldsymbol{y}). \tag{2.8}$$

It may be shown (see, e.g., [1]) that g, defined in (2.3) in terms of Ψ satisfies the normalization condition (in case of a homogeneous system):

$$I_N = \varrho \int d\boldsymbol{r}[1 - g(r)] = 1. \tag{2.9}$$

In case of a non-interacting system, we denote the radial distribution function by g_0. We have

$$g_0(r) = 1 - l(k_F r)^2/v, \tag{2.10}$$

where

$$l(x) = 3j_1(x)/x. \tag{2.11}$$

Normalization condition (2.9) is satisfied by g_0,

$$\varrho \int d\boldsymbol{r}[1 - g_0(r)] = 1, \tag{2.12}$$

and we may write (2.9) as

$$\varrho \int d\boldsymbol{r}[g_0(r) - g(r)] = 0. \tag{2.13}$$

If we know G or g we may easily calculate the expectation value of any two-body operator, Eq. (2.6):

$$\langle W \rangle = \tfrac{1}{2} \int d\boldsymbol{r}_1 d\boldsymbol{r}_2 G(\boldsymbol{r}_1, \boldsymbol{r}_2) w(r_{12}), \tag{2.14}$$

or

$$\langle W \rangle / N = \tfrac{1}{2} \varrho \int d\boldsymbol{r} g(r) w(r). \tag{2.15}$$

3. Perturbation expansion of g

To simplify the presentation, we disregard spin and isospin in all our general derivations, i.e., we put $v = 1$. We assume that the two-body interaction

$$V = \sum_{i<j} \sum v(r_{ij}) \tag{3.1}$$

is of a pure Wigner type, i.e., it does not depend on spin and isospin. In this case the modification of our considerations for $v > 1$ is obvious, and our results for a general spin-isospin degeneracy are presented in Section 8.

In calculating the radial distribution function, we shall use the identity

$$G(x, y) = \langle \tilde{W} \rangle, \tag{3.2}$$

where $\tilde{W}$ is the two-body operator of Eq. (2.8). The method of calculating the expectation value of any two-body operator W, Eq. (2.6), in the perturbation theory is well known (see, e.g., the textbook by Fetter and Walecka [6]).

The best way of showing the perturbation series is by means of diagrams. We illustrate it in Fig. 1 which contains all terms of $\langle W \rangle$ of zero and first order in v, denoted by $\langle W \rangle^{(0)}$ and $\langle W \rangle^{(1)}$ respectively. The double horizontal line represents the two-body operator w, the broken horizontal line represents the two-body interaction v, and the up- (down-)

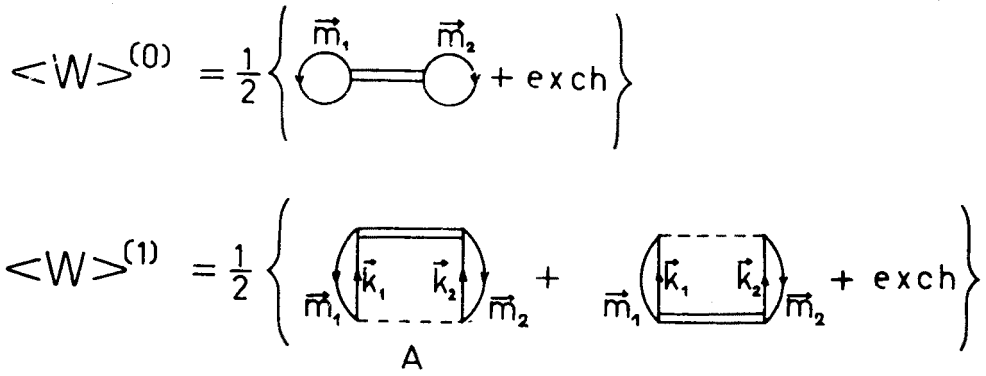

Fig. 1. Diagrams that contribute to the expectation value of a two-body operator W

going lines represent particles (holes). Throughout this paper, the momentum of the i-th particle is denoted by $\boldsymbol{k}_i$, and the momentum of the i-th hole is denoted by $\boldsymbol{m}_i$, i.e., we have $k_i > k_F$, and $m_i \leqslant k_F$. (Otherwise momenta are denoted in general by $\boldsymbol{p}_i$.)

The contribution of the diagram A in Fig. 1 to $\langle W \rangle^{(1)}$ is

$$\langle W \rangle_A^{(1)} = \sum_{\boldsymbol{m}_1 \boldsymbol{m}_2 \boldsymbol{k}_1 \boldsymbol{k}_2} (\phi_{\boldsymbol{m}_1 \boldsymbol{m}_2} | w | \phi_{\boldsymbol{k}_1 \boldsymbol{k}_2}) \left[\varepsilon_{m_1} + \varepsilon_{m_2} - \varepsilon_{k_1} - \varepsilon_{k_2}\right]^{-1} (\phi_{\boldsymbol{k}_1 \boldsymbol{k}_2} | v | \phi_{\boldsymbol{m}_1 \boldsymbol{m}_2}), \tag{3.3}$$

where ε_{p_i} denotes the single-particle kinetic energy,

$$\varepsilon_{pi} = p_i^2 / 2\mathcal{M}, \tag{3.4}$$

where $\mathcal{M}$ is the mass of the particle divided by $\hbar^2$. By $|\phi_{p_1 p_2})$ we denote the product of two single-particle momentum states,

$$|\phi_{p_1 p_2}) = |\varphi_{p_1})\,|\varphi_{p_2}), \tag{3.5}$$

or in coordinate space representation,

$$\begin{aligned}(r_1 r_2|\phi_{p_1 p_2}) &= \phi_{p_1 p_2}(r_1 r_2) = (r_1|\varphi_{p_1})\,(r_2|\varphi_{p_2}) = \varphi_{p_1}(r_1)\varphi_{p_2}(r_2)\\ &= [\exp(r_1 p_1)/\sqrt{Q}]\,[\exp(r_2 p_2)/\sqrt{Q}].\end{aligned} \tag{3.6}$$

By applying the results for $\langle W\rangle^{(0)}$ and $\langle W\rangle^{(1)}$ to the case $W = \tilde{W}$, we obtain the zero and first order (in v) parts of G shown in Fig. 2. We represent $\tilde{w}/2$ by the heavy hori-

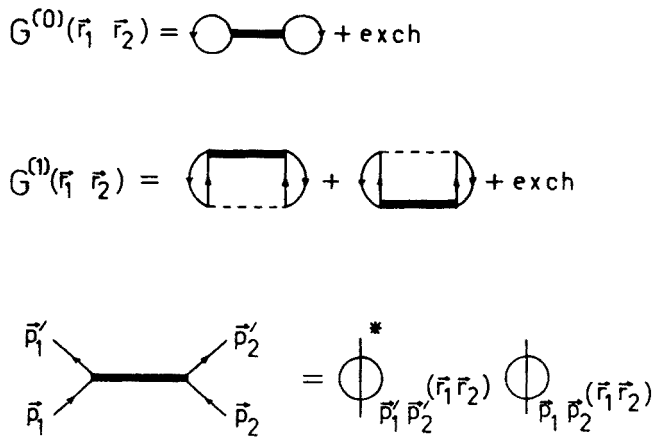

Fig. 2. Diagrams that contribute to $G^{(0)}$ and $G^{(1)}$

zontal line, and consequently the heavy horizontal line together with the in- and out-going particle lines represents the product of plane-wave states, shown on the bottom of Fig. 2. Obviously, we have $G^{(0)} = \varrho^2 g_0$, where g_0 is given in Eq. (2.10).

To obtain the expectation value $\langle V\rangle$ of the two-body interaction, we apply Eq. (2.14) with $w = v$. In this way, if we know G with an accuracy $\sim v^n$, we obtain $\langle V\rangle$ with an accuracy $\sim v^{n+1}$. The diagrammatical rule is here that we replace the heavy $\tilde{w}$-lines by broken v-lines in all G-diagrams, and introduce an extra factor 1/2. In this way, with the help of $G^{(0)}$ and $G^{(1)}$, Fig. 2, we obtain the first and second order expressions for $\langle V\rangle$, $\langle V\rangle^{(1)}$ and $\langle V\rangle^{(2)}$.

The whole procedure may be extended to higher orders in v where, however, the number of diagrams increases rapidly. And the problem arises of selecting those diagrams which are most important in a given physical situation.

4. Low density approximation

In the case of a strong two-body interaction, especially in the presence of hard core repulsion, the perturbation expansion becomes meaningless. In our calculation of the radial distribution function, we follow the systematic approach in terms of hole lines, in

which we group the contributions (G-diagrams) according to the number of interacting particles (number of hole lines). Since each independent hole line introduces into the expectation value of a two-body operator a factor proportional to $k_F^3 \sim \varrho$, the wole line expansion is expected to be an expansion in the density ϱ.

The starting point of the expansion is the low density (LD) approximation, in which only diagrams with two hole lines are considered. To obtain the LD approximation of G,

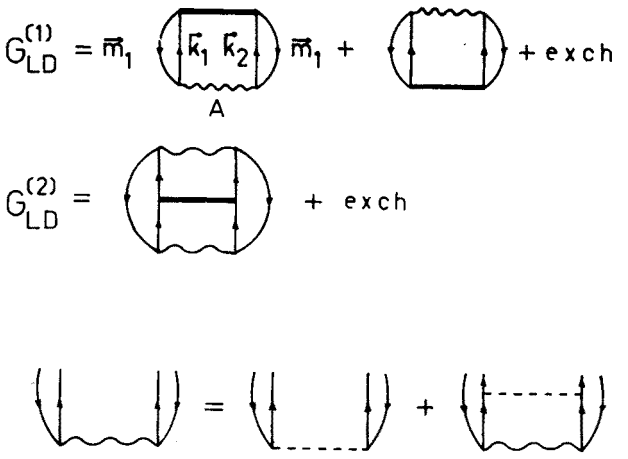

Fig. 3. Diagrams that contribute to $G_{LD}{}^{(1)}$ and $G_{LD}{}^{(2)}$

G_{LD}, we add to $G^{(1)}$ in Fig. 1 diagrams in which v (the broken line) is replaced by particle--ladders of v. Furthermore, we introduce diagrams of the second order in v with two hole lines and add to them the diagrams with ladders of v. In this way, we obtain for G_{LD}:

$$G_{LD} = G^{(0)} + G_{LD}{}^{(1)} + G_{LD}{}^{(2)}, \tag{4.1}$$

where $G_{LD}{}^{(1)}$ and $G_{LD}{}^{(2)}$ are represented diagrammatically in Fig. 3. By a wavy line, we represent the sum of all ladders of v, i.e., the (on-shell) K matrix which satisfies the equation (represented diagrammatically on the bottom of Fig. 3)

$$K|\phi_{m_1m_2}) = v|\phi_{m_1m_2}) + \sum_{k_1k_2} v|\phi_{k_1k_2}) \left[\varepsilon_{m_1} + \varepsilon_{m_2} - \varepsilon_{k_1} - \varepsilon_{k_2}\right]^{-1} (\phi_{k_1k_2}|K|\phi_{m_1m_2}). \tag{4.2}$$

For the wave function $\psi_{m_1m_2}$ of two interacting particles, defined by

$$K|\phi_{m_1m_2}) = v|\psi_{m_1m_2}), \tag{4.3}$$

we get from (4.2) the equation:

$$|\psi_{m_1m_2}) - |\phi_{m_1m_2}) \equiv |\chi_{m_1m_2}) = \sum_{k_1k_2} |\phi_{k_1k_2}) \left[\varepsilon_{m_1} + \varepsilon_{m_2} - \varepsilon_{k_1} - \varepsilon_{k_2}\right]^{-1} (\phi_{k_1k_2}|K|\phi_{m_1m_2}). \tag{4.4}$$

As an example, let us calculate the contribution $G_{LD(A)}{}^{(1)}$ of diagram A in Fig. 3. We have:

$$\begin{aligned} G_{LD(A)}{}^{(1)} &= \sum_{m_1m_2k_1k_2} \phi^*_{m_1m_2}(r_1r_2)\phi_{k_1k_2}(r_1r_2) \left[\varepsilon_{m_1} + \varepsilon_{m_2} - \varepsilon_{k_1} - \varepsilon_{k_2}\right]^{-1} (\phi_{k_1k_2}|K|\phi_{m_1m_2}) \\ &= \sum_{m_1m_2} \phi^*_{m_1m_2}(r_1r_2)\chi_{m_1m_2}(r_1r_2). \end{aligned} \tag{4.5}$$

In the last step in Eq. (4.5), we used Eq. (4.4), and the notation:

$$\chi_{m_1m_2}(r_1r_2) = (r_1r_2|\chi_{m_1m_2}) = (r_1r_2|\psi_{m_1m_2})$$
$$-(r_1r_2|\phi_{m_1m_2}) = \psi_{m_1m_2}(r_1r_2) - \phi_{m_1m_2}(r_1r_2). \tag{4.6}$$

Proceeding in the same way with all the other contributions to G_{LD}, we get:

$$G^{(0)} = \sum_{m_1m_2} \phi^*_{m_1m_2}(r_1r_2)\,[\phi_{m_1m_2}(r_1r_2) - \phi_{m_2m_1}(r_1r_2)], \tag{4.7}$$

$$G_{\mathrm{LD}}{}^{(1)} = \sum_{m_1m_2} \phi^*_{m_1m_2}(r_1r_2)\,[\chi_{m_1m_2}(r_1r_2) - \chi_{m_2m_1}(r_1r_2)] + \text{c.c.}, \tag{4.8}$$

$$G_{\mathrm{LD}}{}^{(2)} = \sum_{m_1m_2} \chi^*_{m_1m_2}(r_1r_2)\,[\chi_{m_1m_2}(r_1r_2) - \chi_{m_2m_1}(r_1r_2)]. \tag{4.9}$$

By adding these expressions we get, with the help of relation (4.6), our final result for G_{LD}:

$$G_{\mathrm{LD}}(r_1r_2) = \sum_{m_1m_2} \psi^*_{m_1m_2}(r_1r_2)\,[\psi_{m_1m_2}(r_1r_2) - \psi_{m_2m_1}(r_1r_2)]. \tag{4.10}$$

5. *Normalization condition*

Let us first write the normalization condition for the radial distribution function, Eq. (2.13), in the form:

$$\varrho \int dr_1 dr_2 [G^{(0)}(r_1r_2) - G(r_1r_2)] = 0. \tag{5.1}$$

In the LD approximation, $G \cong G_{\mathrm{LD}}$, Eq. (4.1), condition (5.1) is not satisfied exactly. Namely, we have:

$$\varrho \int dr_1 dr_2 [G^{(0)} - G_{\mathrm{LD}}] = -\varrho \int dr_1 dr_2 [G_{\mathrm{LD}}{}^{(1)} + G_{\mathrm{LD}}{}^{(2)}] = -\varrho \int dr_1 dr_2 G_{\mathrm{LD}}{}^{(2)}. \tag{5.2}$$

The last step in Eq. (5.2) follows from expression (4.8) for $G_{\mathrm{LD}}{}^{(1)}$. (Since $\chi_{m_1m_2}$ has non-vanishing components only for single-particle momenta greater than the Fermi momentum (see Eq. (4.4)) it is orthogonal to $\phi_{m_1m_2}$, and consequently the contribution of $G_{\mathrm{LD}}{}^{(1)}$ to the normalization integral vanishes).

So far all the wave functions have been normalized in a box of volume Ω. For instance (see Eq. (3.6)),

$$\phi_{p_1p_2}(r_1r_2) = \exp[i(p_1r_1 + p_2r_2)]/\Omega = [\exp(i\boldsymbol{PR})/\Omega] \exp(i\boldsymbol{pr}), \tag{5.3}$$

where $\boldsymbol{P} = \boldsymbol{p}_1 + \boldsymbol{p}_2$ is the CM momentum, $\boldsymbol{p} = (\boldsymbol{p}_2 - \boldsymbol{p}_1)/2$ is the relative momentum, $\boldsymbol{R} = (r_1 + r_2)/2$ is the CM coordinate, and $r = r_2 - r_1$ is the relative coordinate. With the help of the notation

$$\phi_p(r) = \exp(ipr), \tag{5.4}$$

we may write (5.3) in the form:

$$\phi_{p_1p_2}(r_1r_2) = \Omega^{-1}\phi_P(\boldsymbol{R})\phi_p(\boldsymbol{r}). \tag{5.5}$$

Similarly, we introduce the notation:

$$\psi_{m_1 m_2}(r_1 r_2) = \Omega^{-1}\phi_M(R)\psi_m{}^M(r), \tag{5.6}$$

$$\chi_{m_1 m_2}(r_1 r_2) = \Omega^{-1}\phi_M(R)\chi_m{}^M(r). \tag{5.7}$$

Notice that the functions $\psi_m{}^M$ and $\chi_m{}^M$ depend not only on the relative momentum $\boldsymbol{m} = (\boldsymbol{m}_2 - \boldsymbol{m}_1)/2$ but also on the CM momentum $\boldsymbol{M} = \boldsymbol{m}_1 + \boldsymbol{m}_2$, in contradistinction to the function ϕ_p (Eq. (5.4)), which depends only on the relative momentum.

Using wave functions of relative motion $\psi_m{}^M$ and the difference functions $\chi_m{}^M$, we can rewrite Eq. (5.2) in the form:

$$\varrho \int d\boldsymbol{r}[g_0(r) - g_{\mathrm{LD}}(r)] = -\kappa, \tag{5.8}$$

where $\varrho^2 g_{\mathrm{LD}} = G_{\mathrm{LD}}$, and κ is the average value (in the Fermi sea) of the wound integral:

$$\kappa = \kappa_{\mathrm{D}} - \kappa_{\mathrm{Ex}} = N^{-2} \sum_{m_1 m_2} \varrho \int d\boldsymbol{r} \chi_m{}^M(r)^* [\chi_m{}^M(r) - \chi_{-m}{}^M(r)]. \tag{5.9}$$

(By κ_{D} and κ_{Ex}, we denote the direct and exchange part of κ.) The corresponding value of the normalization integral I_N, Eq. (2.9), is

$$I_N = 1 - \kappa. \tag{5.10}$$

Since κ appears to play the role of a smallness parameter in the hole line expansion, we may say that the normalization condition, Eq. (2.13), is satisfied within the accuracy of the LD approximation.

The normalization condition, Eq. (2.13), follows from the fact that the exact radial distribution function is expressed with the help of the N-body wave function Ψ, Eq. (2.3). To construct the radial distribution function which satisfies the normalization condition *exactly*, we must therefore first define Ψ in some given approximation, and then calculate the complete radial distribution function with this Ψ.

In the case of the LD approximation, we introduce the approximate form of Ψ, denoted by Ψ_{LD}, which is represented diagrammatically in Fig. 4 (Φ denotes the ground state wave

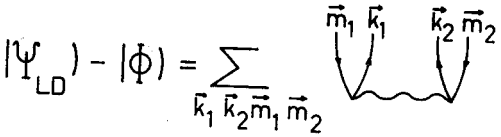

Fig. 4. Diagrammatical representation of ψ_{LD}

function of the noninteracting system). If we use this Ψ_{LD} to calculate the radial distribution function $G'_{\mathrm{LD}} = \varrho^2 g'_{\mathrm{LD}}$ according to Eq. (2.3), we get

$$G'_{\mathrm{LD}} = G_{\mathrm{LD}} + G'_{\mathrm{LD}}{}^{(2)}, \tag{5.11}$$

where $G'_{\mathrm{LD}}{}^{(2)}$ is represented diagrammatically in Fig. 5. It is easy to check that g'_{LD} does indeed satisfy the normalization condition, Eq. (2.9), *exactly*. Notice that the parts of

$G'_{LD}{}^{(2)}$ denoted in Fig. 5 by d, e, n, o give zero contribution to the normalization integral I_N, Eq. (2.9).

However, g'_{LD} is *not* a consistent approximation to the radial distribution function in the sense of the hole-line expansion. It differs from g_{LD} by terms which involve three

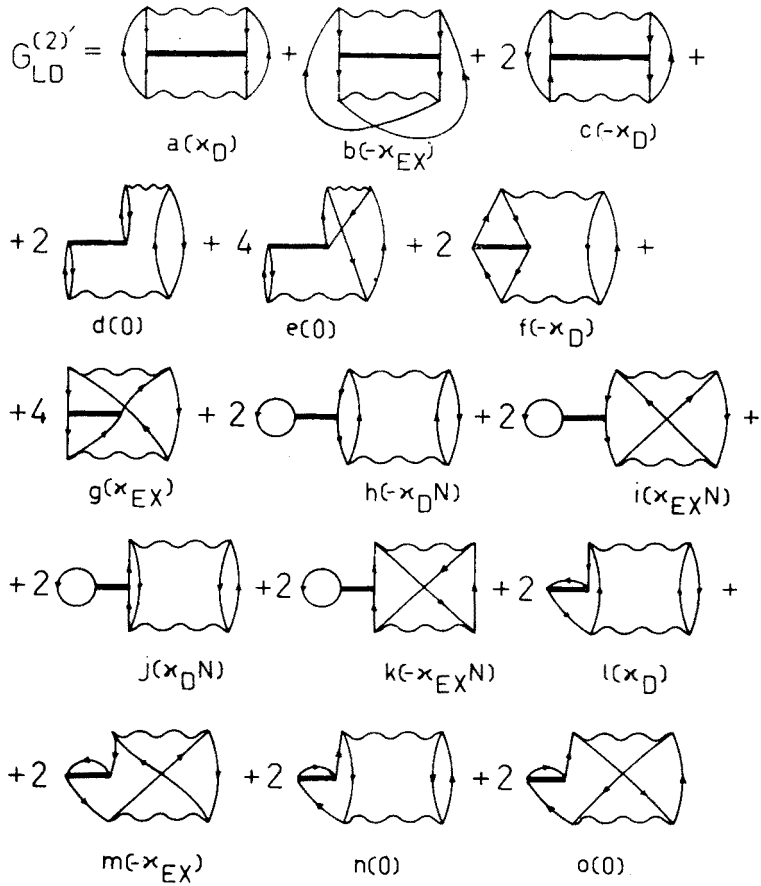

Fig. 5. Diagrams that contribute to $G'_{LD}{}^{(2)}$. The contribution of each diagram to $-I_N$, Eq. (2.9), is given in parentheses

independent hole lines. However, there are several other G-diagrams with three hole lines beyond those shown in Fig. 5. Notice that if we used G'_{LD} to calculate $\langle V \rangle$, we would obtain an infinite result in case of two-body interaction with a hard core.

6. *The potential energy*

With the help of G_{LD}, we may calculate in the LD approximation the potential energy, i.e., the expectation value of the two-body interaction,

$$\langle V \rangle_{LD} = \tfrac{1}{2} \int dr_1 dr_2 G_{LD}(r_1 r_2) v(r_{12}) = \tfrac{1}{2} \sum_{m_1 m_2} (\psi_{m_1 m_2} | v | \psi_{m_1 m_2} - \psi_{m_2 m_1}). \qquad (6.1)$$

Following the prescription described at the end of Section 3, we obtain for $\langle V\rangle_{\mathrm{LD}}$ the result shown in Fig. 6. The last step in the diagrammatic equation in Fig. 6 follows from the definition of the K matrix, Eq. (4.2).

Notice that the part of $\langle V\rangle_{\mathrm{LD}}$, denoted by A in Fig. 6, is the LD approximation ΔE_{LD} of $\Delta E = E - E_0$, where E is the total ground state energy of the interacting system,

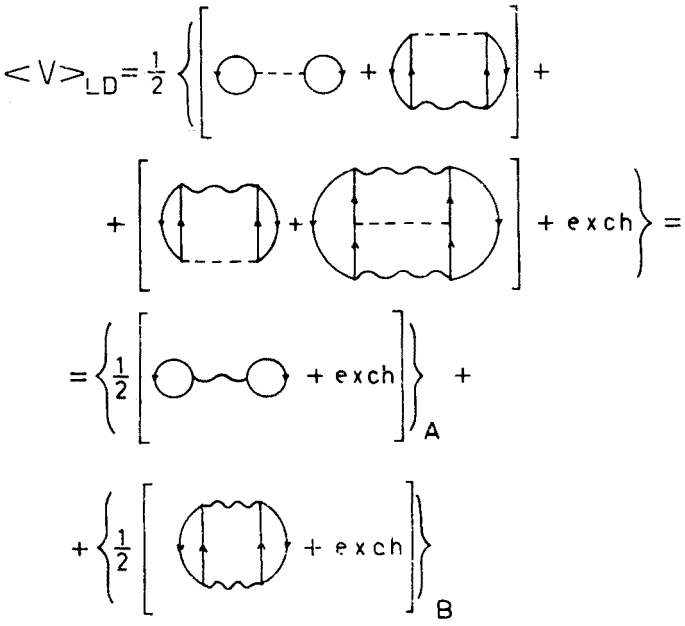

Fig. 6. Diagrammatical representation of $\langle V\rangle_{\mathrm{LD}}$

and $E_0 = \frac{3}{5}\varepsilon_{k_F}N$. To repeat: ΔE_{LD} is the ladder-approximation to the energy. It is the two-hole line expansion without insertions in hole- or particle-lines,

$$\Delta E_{\mathrm{LD}} = \tfrac{1}{2}\sum_{m_1 m_2}(\phi_{m_1 m_2}|K|\phi_{m_1 m_2} - \phi_{m_2 m_1}) = \tfrac{1}{2}\sum_{m_1 m_2}(\phi_{m_1 m_2}|v|\psi_{m_1 m_2} - \psi_{m_2 m_1}). \tag{6.2}$$

Consequently, we have

$$\langle V\rangle_{\mathrm{LD}} = \Delta E_{\mathrm{LD}} + X_{\mathrm{B}}, \tag{6.3}$$

where X_{B} is represented by the B diagrams in Fig. 6,

$$X_{\mathrm{B}} = \tfrac{1}{2}\sum_{k_1 k_2 m_1 m_2}(\phi_{m_1 m_2}|K|\phi_{k_1 k_2})\,[\varepsilon_{m_1} + \varepsilon_{m_2} - \varepsilon_{k_1} - \varepsilon_{k_2}]^{-1}\,(\phi_{k_1 k_2}|K|\phi_{m_1 m_2} - \phi_{m_2 m_1})$$

$$= \tfrac{1}{2}\sum_{m_1 m_2}(\chi_{m_1 m_2}|K|\phi_{m_1 m_2} - \phi_{m_2 m_1}) = \tfrac{1}{2}\sum_{m_1 m_2}(\chi_{m_1 m_2}|v|\psi_{m_1 m_2} - \psi_{m_2 m_1}), \tag{6.4}$$

where the last two steps have been accomplished with the help of Eqs. (4.4) and (4.3).

It is essential for the consistency of our whole approach, that we should obtain the LD approximation to the total energy, E_{LD}, if we add to $\langle V\rangle_{\mathrm{LD}}$ the LD approximation of the expectation value of the kinetic energy, $\langle T\rangle_{\mathrm{LD}}$.

7. *The kinetic energy*

The calculation of the expectation value of the kinetic energy, $\langle T\rangle$, follows the known rules of calculating the expectation value of a one-body operator (see, e.g., the textbook by Thouless [7]). The result is best represented by diagrams. We illustrate it in Fig. 7 which contains all terms of $\langle T\rangle$ of zero and of second order in v, denoted by $\langle T\rangle^{(0)}$ and

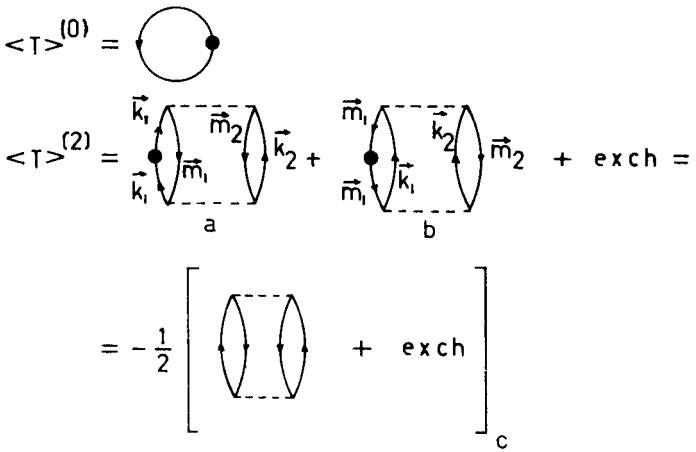

Fig. 7. Diagrams that contribute to $\langle T\rangle^{(0)}$ and $\langle T\rangle^{(2)}$

$\langle T\rangle^{(2)}$ respectively (notice that $\langle T\rangle^{(1)} = 0$). By a heavy dot on a p_i-line, we denote the diagonal matrix element of the kinetic energy of the i-th particle, ε_{p_i}. Otherwise the usual diagrammatical rules obey, and we have:

$$\langle T\rangle^{(0)} = E_0 = T_0 = \sum_{m_1} \varepsilon_{m_1} = \tfrac{3}{5}\,\varepsilon_{k_F} N, \tag{7.1}$$

$$\langle T\rangle^{(2)} = \sum_{k_1 k_2 m_1 m_2} (\phi_{m_1 m_2}|v|\phi_{k_1 k_2})\,[\varepsilon_{m_1}+\varepsilon_{m_2}-\varepsilon_{k_1}-\varepsilon_{k_2}]^{-1}$$

$$\times\,[\varepsilon_{k_1}-\varepsilon_{m_1}]\,[\varepsilon_{m_1}+\varepsilon_{m_2}-\varepsilon_{k_1}-\varepsilon_{k_2}]^{-1}\,(\phi_{k_1 k_2}|v|\phi_{m_1 m_2}-\phi_{m_2 m_1})$$

$$= -\tfrac{1}{2}\sum_{k_1 k_2 m_1 m_2} (\phi_{m_1 m_2}|v|\phi_{k_1 k_2})\,[\varepsilon_{m_1}+\varepsilon_{m_2}-\varepsilon_{k_1}-\varepsilon_{k_2}]^{-1}\,(\phi_{k_1 k_2}|v|\phi_{m_1 m_2}-\phi_{m_2 m_1}). \tag{7.2}$$

Notice the additional minus sign of the contribution of the diagram b in Fig. 7 (and consequently the minus sign at ε_{m_1} in (7.2)), connected with three hole lines (two m_1-lines and one m_2-line). The result of the last step in Eq. (7.2) is represented as diagrams c in Fig. 7.

In the LD approximation, we consider all diagrams with two hole lines. The sum of all these diagrams is obtained by replacing in $\langle T\rangle^{(2)}$ the interaction v by the K matrix. In this way we obtain for the LD approximation of $\langle T\rangle$, $\langle T\rangle_{\mathrm{LD}}$, the result shown in Fig. 8. The last step in Fig. 8 is accomplished similarly as in the case of $\langle T\rangle^{(2)}$.

A comparison of the results for $\langle T\rangle_{LD}$ in Fig. 8 and for $\langle T\rangle_{LD}$ in Fig. 6 leads to the following expression for $\langle T\rangle_{LD}$:

$$\langle T\rangle_{LD} = E_0 - X_B, \tag{7.3}$$

where X_B, given by expression (6.7), is represented by the B diagrams in Fig. 8 or Fig. 6.

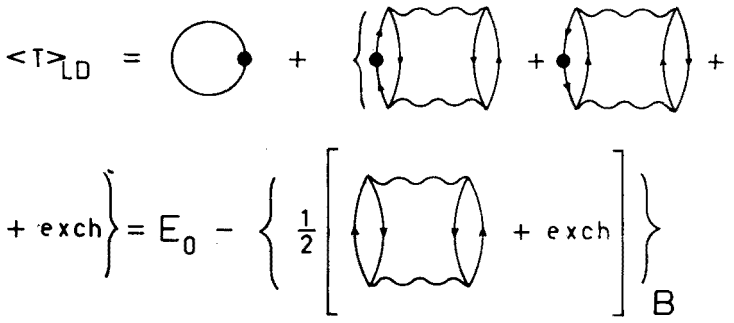

Fig. 8. Diagrammatical representation of $\langle T\rangle_{LD}$

By adding the expressions for $\langle V\rangle_{LD}$, Eq. (6.2), and for $\langle T\rangle_{LD}$, Eq. (7.3), we get

$$\langle T\rangle_{LD} + \langle V\rangle_{LD} = E_0 + \Delta E_{LD}. \tag{7.4}$$

We thus find that in the LD limit the total energy calculated from the perturbation expansion of the radial distribution function, and of the kinetic energy, is identical to the known perturbation expansion of the total energy, $E_0 + \Delta E_{LD}$. Essential is of course that the similar diagrams are included in both cases. The result is to be considered as a consistency-check.

An approximate result, similar to Eq. (7.4), was obtained in a different context by Wong [8].

8. LD approximation — calculational procedure

A. Wigner forces

So far we have not taken into account spin and isospin, i.e., we put $v = 1$. In the case of Wigner forces, it is straightforward to modify all our equations for a general spin-isospin degeneracy v. The modifications amount to multiplying all summations over $\boldsymbol{m}_i$ by v, and all exchange terms by $1/v$. For instance, Eq. (4.10) for G_{LD} takes the form:

$$G_{LD}(\boldsymbol{r}_1\boldsymbol{r}_2) = v^2 \sum_{m_1 m_2} \psi^*_{m_1 m_2}(\boldsymbol{r}_1\boldsymbol{r}_2)\,[\psi_{m_1 m_2}(\boldsymbol{r}_1\boldsymbol{r}_2) - \psi_{m_2 m_1}(\boldsymbol{r}_1\boldsymbol{r}_2)/v]. \tag{8.1}$$

We solve the K matrix equation, Eq. (4.2), or equivalently the wave function equation, Eq. (4.4), in configuration space. We introduce the wave function $\psi_m{}^M(\boldsymbol{r})$ of the relative motion of two particles, Eq. (5.6), and the difference function (see Eq. (5.7))

$$\chi_m{}^M(\boldsymbol{r}) = \psi_m{}^M(\boldsymbol{r}) - \phi_m(\boldsymbol{r}). \tag{8.2}$$

Wave function equation (4.4) takes the form:

$$\psi_m{}^M(\boldsymbol{r}) = \phi_m(\boldsymbol{r}) + \int d\boldsymbol{r}' \mathcal{G}^{Mm}(\boldsymbol{r}\boldsymbol{r}') v(r') \psi_m{}^M(\boldsymbol{r}'), \tag{8.3}$$

where we have introduced the Green function

$$\mathcal{G}^{Mm}(\boldsymbol{r}\boldsymbol{r}') = \mathcal{M}(2\pi)^{-3} \int d\boldsymbol{k} [Q(M, k)/(m^2 - k^2)] e^{i\boldsymbol{k}(\boldsymbol{r}-\boldsymbol{r}')}. \tag{8.4}$$

Here, we have approximated the exclusion principle operator by its angle average

$$Q(M, k) = \begin{cases} 0 & \text{for} \quad k < (k_F^2 - M^2/4)^{1/2}, \\ 1 & \text{for} \quad k > k_F + M/2, \\ (k^2 - k_F^2 + M^2/4)/kM & \text{otherwise.} \end{cases} \tag{8.5}$$

Notice that because of approximation (8.5), the wave function $\psi_m{}^M$ and the Green function $\mathcal{G}^{Mm}$ do not depend on the direction of $\boldsymbol{M}$, but only on its absolute value.

With the partial wave decomposition,

$$\psi_m{}^M(\boldsymbol{r}) = \sum_l i^l \sqrt{4\pi(2l+1)}\, Y_{l0}(\hat{\boldsymbol{m}}\hat{\boldsymbol{r}}) u_l^M(m, r), \tag{8.6}$$

$$\mathcal{G}^{Mm}(\boldsymbol{r}\boldsymbol{r}') = \sum_l \sqrt{4\pi(2l+1)}\, Y_{l0}(\hat{\boldsymbol{r}}\hat{\boldsymbol{r}}') \mathcal{G}_l^{Mm}(rr'), \tag{8.7}$$

$$\mathcal{G}_l^{Mm}(rr') = (\mathcal{M}/2\pi^2) \int_0^\infty dk k^2 [Q(M, k)/(m^2 - k^2)] j_l(kr) j_l(kr'), \tag{8.8}$$

Eq. (8.3) takes the form:

$$u_l^M(m, r) = j_l(mr) + 4\pi \int_0^\infty dr' r'^2 \mathcal{G}_l^{Mm}(rr') v(r') u_l^M(m, r'). \tag{8.9}$$

(Our method of calculating $\mathcal{G}_l^{Mm}$ is shown in Appendix A.)

For the integration over the momenta in the Fermi sea, we use the formulas:

$$\int d\boldsymbol{M} \int d\boldsymbol{m} f(\boldsymbol{m}, M) = (\tfrac{4}{3}\pi k_F^3)^2 \hat{\mathcal{I}}_{mM} \bar{f}(m, M), \tag{8.10}$$

$$\int d\boldsymbol{M} \int d\boldsymbol{m} f(\boldsymbol{m}) = (\tfrac{4}{3}\pi k_F^3)^2 \hat{\mathcal{I}}_m \bar{f}(m), \tag{8.11}$$

where angle averaging is denoted by bars, e.g.,

$$\bar{f}(m, M) = \int d\hat{\boldsymbol{m}} f(\boldsymbol{m}, M)/4\pi, \tag{8.12}$$

and where the integration operators $\hat{\mathcal{I}}$ are:

$$\hat{\mathcal{I}}_{mM} = 9 \int_0^1 d\tilde{m}\tilde{m} \{\tilde{m} \int_0^{2(1-\tilde{m})} d\tilde{M}\tilde{M}^2 + \int_{2(1-\tilde{m})}^{2\sqrt{1-\tilde{m}^2}} d\tilde{M}\tilde{M}(1 - \tilde{m}^2 - \tilde{M}^2/4)\}, \tag{8.13}$$

$$\hat{\mathcal{I}}_m = 24 \int_0^1 d\tilde{m}\tilde{m}^2 (1 - \tfrac{3}{2}\tilde{m}^2 + \tfrac{1}{2}\tilde{m}^3), \tag{8.14}$$

where $\tilde{m} = m/k_F$ and $\tilde{M} = M/k_F$.

With the partial wave decomposition, Eq. (8.6), we may write Eq. (8.1) in the form:

$$g_{\mathrm{LD}}(r) = \hat{\mathscr{I}}_{mM} \sum_l (2l+1)\,[1-(-)^l/v]\,|u_l^M(m, r)|^2. \tag{8.15}$$

By replacing u_l^M by j_l in (8.15), we get

$$g_0(r) = \hat{\mathscr{I}}_m \sum_l (2l+1)\,[1-(-)^l/v] j_l(mr)^2 = \hat{\mathscr{I}}_m\{1-j_0(2mr)/v\} = 1-l(k_{\mathrm{F}}r)^2/v. \tag{8.16}$$

For the expectation value of V (see Eq. (6.1)) and T (see Eqs (7.3), (6.7)) we have:

$$\langle V\rangle_{\mathrm{LD}}/N = \tfrac{1}{2}\varrho \int dr g_{\mathrm{LD}}(r) v(r)$$

$$= \tfrac{1}{2}\varrho \hat{\mathscr{I}}_{mM} \sum_l (2l+1)\,[1-(-)^l/v] 4\pi \int_0^\infty dr r^2 u_l^M(m, r) v(r) u_l^M(m, r), \tag{8.17}$$

$$\langle T\rangle_{\mathrm{LD}}/N = \tfrac{3}{5}\varepsilon_{k_{\mathrm{F}}} - \tfrac{1}{2}\varrho \hat{\mathscr{I}}_{mM} \sum_l (2l+1)\,[1-(-)^l/v]$$

$$\times 4\pi \int_0^\infty dr r^2 [u_l^M(m, r) - j_l(mr)] v(r) u_l^M(m, r). \tag{8.18}$$

If the two-body potential has a hard core of radius c, and is equal to $v(r)$ for $r > c$, we replace the hard core by a hard shell with the same radius c (see, e.g., [9]). Wave equation (8.9) then takes the form:

$$u_l^M(m, r) = s_l^M(m, r) + 4\pi \int_c^\infty dr' r'^2 \mathscr{F}_l^{Mm}(rr') v(r') u_l^M(m, r'), \tag{8.19}$$

where

$$s_l^M(m, r) = j_l(mr) - j_l(mc)\mathscr{G}_l^{Mm}(rc)/\mathscr{G}_l^{Mm}(cc), \tag{8.20}$$

$$\mathscr{F}_l^{Mm}(rr') = \mathscr{G}_l^{Mm}(rr') - \mathscr{G}_l^{Mm}(rc)\mathscr{G}_l^{Mm}(cr')/\mathscr{G}_l^M(cc). \tag{8.21}$$

In place of Eq. (8.18), we now have:

$$\langle T\rangle_{\mathrm{LD}}/N = \tfrac{3}{5}\varepsilon_{k_{\mathrm{F}}} - \tfrac{1}{2}\varrho \hat{\mathscr{I}}_{mM} \sum_l (2l+1)\,[1-(-)^l/v]$$

$$\times \{j_l(mc)^2/\mathscr{G}_l^{Mm}(cc) + 4\pi \int_c^\infty dr r^2 [u_l^M(m, r) - s_l^M(m, r)] v(r) u_l^M(m, r). \tag{8.22}$$

Notice that expression (8.17) for $\langle V\rangle_{\mathrm{LD}}$ remains unchanged (since $uvu = 0$ for $r < c$, we may now replace in (8.17) the lower zero limit in the r-integration by c).

B. Spin-isospin dependent forces

Let us first consider nuclear matter for which $v = 4$. There are $v = 4$ spin–isospin two-body states (S, T) which we denote by $\lambda = 1, \ldots, v$. The $\lambda = 1$ state is the spin singlet–isospin singlet state $(0, 0)$, $\lambda = 2$ is the spin singlet-isospin triplet state $(0, 1)$, $\lambda = 3$ is the $(1, 0)$ state, and $\lambda = 4$ is the $(1, 1)$ state. The projection operators onto these states are denoted by Λ^λ, e.g.,

$$\Lambda_{12}^{\lambda=3} = \tfrac{1}{16}(3+\boldsymbol{\sigma}_1\boldsymbol{\sigma}_2)(1-\boldsymbol{\tau}_1\boldsymbol{\tau}_2). \tag{8.23}$$

The two-body interaction considered here has the form

$$\hat{v}_{12} = \sum_{\lambda} v_{\lambda}(r_{12}) \Lambda_{12}^{\lambda}, \tag{8.24}$$

which implies that the K matrix has the analogous form,

$$\hat{K} = \sum_{\lambda} K_{\lambda} \Lambda_{12}^{\lambda}, \tag{8.25}$$

where K_{λ} satisfies Eq. (4.2) with v replaced by v_{λ}. Functions ψ and χ are now different in different spin–isospin states, and are denoted by ψ^{λ} and χ^{λ}, where ψ^{λ} is defined by Eq. (4.3) with v and K replaced by v_{λ} and K_{λ}, and χ^{λ} by a similarly modified Eq. (4.4).

To calculate the expectation value of the interaction, or of any other spin–isospin dependent two-body operator, we introduce the radial distribution function $G^{\lambda} = \varrho^2 g^{\lambda}$ for the spin–isospin state λ:

$$d_{\lambda} G^{\lambda}(\boldsymbol{r}_1 \boldsymbol{r}_2) = N(N-1) \int d\xi_1 d\xi_2 d\boldsymbol{r}_3 d\xi_3 \ldots d\boldsymbol{r}_N d\xi_N$$
$$\times \Psi^*(\boldsymbol{r}_1 \xi_1 \ldots \boldsymbol{r}_N \xi_N) \Lambda_{12}^{\lambda} \Psi(\boldsymbol{r}_1 \xi_1 \ldots \boldsymbol{r}_N \xi_N) / (\Psi|\Psi), \tag{8.26}$$

where

$$d_{\lambda} = \mathrm{Tr}\, \Lambda_{12}^{\lambda} / v^2 \tag{8.27}$$

is the weight of the λ state. A definition equivalent to (8.26) is (see Eq. (2.8)):

$$d_{\lambda} G^{\lambda}(\boldsymbol{x}\boldsymbol{y}) = \langle \tilde{W}^{\lambda} \rangle, \tag{8.28}$$

$$\tilde{W}^{\lambda} = \sum_{i<j} \sum \tilde{w}(r_{ij}) \Lambda_{ij}^{\lambda}. \tag{8.29}$$

The calculation of G^{λ} follows precisely the calculation of G for Wigner forces presented before provided that v and K are replaced by v_{λ} and K_{λ}. There is only one difference: the previous factor $1/v$ at the exchange terms must be replaced by the factor

$$\varepsilon_{\lambda} = \mathrm{Tr}\, \Lambda_{12}^{\lambda} P_{12} / \mathrm{Tr}\, \Lambda_{12}^{\lambda}, \tag{8.30}$$

where P_{12} is the spin–isospin exchange operator.

In the LD approximation, we have now:

$$G_{\mathrm{LD}}^{\lambda}(\boldsymbol{r}_1 \boldsymbol{r}_2) = v^2 \sum_{m_1 m_2} \psi_{m_1 m_2}^{\lambda}(\boldsymbol{r}_1 \boldsymbol{r}_2)^* [\psi_{m_1 m_2}^{\lambda}(\boldsymbol{r}_1 \boldsymbol{r}_2) - \varepsilon_{\lambda} \psi_{m_2 m_1}^{\lambda}(\boldsymbol{r}_1 \boldsymbol{r}_2)], \tag{8.31}$$

$$\langle V \rangle_{\mathrm{LD}} = \sum_{\lambda} d_{\lambda} \langle V \rangle_{\mathrm{LD}}^{\lambda}, \tag{8.32}$$

$$\langle V \rangle_{\mathrm{LD}}^{\lambda} = \tfrac{1}{2} \int d\boldsymbol{r}_1 d\boldsymbol{r}_2 G_{\mathrm{LD}}^{\lambda}(\boldsymbol{r}_1 \boldsymbol{r}_2) v_{\lambda}(r_{12}). \tag{8.33}$$

Obviously, we have

$$G = \sum_{\lambda} d_{\lambda} G^{\lambda}. \tag{8.34}$$

Now, let us consider a system with $v = 2$, e.g., neutron matter or ^{3}He. Here, we have two λ states: the spin-singlet state $\lambda = 1$ and the spin-triplet state $\lambda = 2$. Instead of Eq.

(8.23), we have, e.g.,

$$\Lambda_{12}^{\lambda=1} = \tfrac{1}{4}(1-\sigma_1\sigma_2). \tag{8.35}$$

Otherwise, all the remaining equations are valid also for $v = 2$.

Values of d_λ and ε_λ for $v = 4$ and $v = 2$ are given in Table I.

TABLE I

Coefficients d_λ and ε_λ

$v = 2$

S	0	1
λ	1	2
d_λ	1/4	3/4
ε_λ	−1	1

$v = 4$

(S, T)	(0,0)	(0,1)	(1,0)	(1,1)
λ	1	2	3	4
d_λ	1/16	3/16	3/16	9/16
ε_λ	1	−1	−1	1

For a noninteracting system, we have

$$g_0(r) = \sum_\lambda d_\lambda g_0{}^\lambda(r), \tag{8.36}$$

$$g_0{}^\lambda(r) = 1-\varepsilon_\lambda l(k_F r)^2. \tag{8.37}$$

The partial wave decomposition of ψ^λ may be performed as in Section 8A:

$$\psi_m{}^M(\mathbf{r})^\lambda = \sum_l \sqrt{4\pi(2l+1)}\, Y_{l0}(\hat{\mathbf{m}}\hat{\mathbf{r}}) u_l{}^M(m, r)^\lambda, \tag{8.38}$$

where functions $u_l{}^\lambda$ satisfy in the presence of a hard core the equations:

$$u_l{}^M(m, r)^\lambda = s_l{}^M(m, r) + 4\pi \int_c^\infty dr' r'^2 \mathscr{F}_l{}^{Mm}(rr') v_\lambda(r') u_l{}^M(m, r')^\lambda. \tag{8.39}$$

For $g_{LD}{}^\lambda$ and $g_0{}^\lambda$, we get the partial wave decompositions:

$$g_{LD}(r)^\lambda = \hat{\mathscr{I}}_{mM} \sum_l (2l+1)\,[1-\varepsilon_\lambda(-)^l]\,|u_l{}^M(m, r)|^2, \tag{8.40}$$

$$g_0(r)^\lambda = \hat{\mathscr{I}}_m \sum_l (2l+1)\,[1-\varepsilon_\lambda(-)^l] j_l(mr)^2 = \hat{\mathscr{I}}_m[1-\varepsilon_\lambda j_0(2mr)] = 1-\varepsilon_\lambda l(k_F r)^2. \tag{8.41}$$

For $\langle V\rangle_{\mathrm{LD}}^{\lambda}$, we obtain:

$$\langle V\rangle_{\mathrm{LD}}^{\lambda}/N = \tfrac{1}{2}\varrho\hat{\mathscr{I}}_{mM}\sum_{l}(2l+1)\left[1-\varepsilon_{\lambda}(-)^{l}\right]$$

$$\times 4\pi\int_{c}^{\infty} drr^{2}u_{l}^{M}(m,r)^{\lambda}v_{\lambda}(r)u_{l}^{M}(m,r). \tag{8.42}$$

The calculation of $\langle T\rangle$ in case of spin–isospin dependent interaction proceeds similarly, and in the LD approximation the result is:

$$\langle T\rangle_{\mathrm{LD}} = \sum_{\lambda} d_{\lambda}\langle T\rangle_{\mathrm{LD}}^{\lambda}, \tag{8.43}$$

$$\langle T\rangle_{\mathrm{LD}}^{\lambda} = \tfrac{3}{5}\varepsilon_{k_{\mathrm{F}}} - \tfrac{1}{2}\varrho\hat{\mathscr{I}}_{mM}\sum_{l}(2l+1)\left[1-\varepsilon_{\lambda}(-)^{l}\right]$$

$$\times\{j_{l}(mc)^{2}/\mathscr{G}_{l}^{Mm}(cc) + 4\pi\int_{c}^{\infty} drr^{2}[u_{l}^{M}(m,r)^{\lambda} - s_{l}^{M}(m,r)]v_{\lambda}(r)u_{l}^{M}(m,r). \tag{8.44}$$

9. LD approximation — results

In the calculations whose results are presented here, the average CM momentum approximation [10] (see Appendix B) was applied.

In all our calculations, we have considered the interaction in S, P, D states only, and for $l > 2$ the wave functions u_l have been approximated by j_l.

Wave function equations (8.19) (or (8.39)) were transformed into systems of inhomogeneous linear equations by approximating the r-integrals by sums with the help of the Gauss quadrature. We introduced into the r-integrals an upper cut-off R, such that $u_l(m,r) \cong j_l(mr)$ for $r > R$. The systems of inhomogeneous linear equations were solved by the Gauss method.

All numerical integrations appearing in our calculations were performed with the help of the Gauss quadrature.

For numerical convenience, we used our equations for a hard core interaction with radius c in all cases considered. In cases of soft-core interactions, c was chosen to be sufficiently small as not to affect our results.

A. Nuclear matter with V_2 potential

The potential V_2 is equal to the central component of the Reid [11] soft core potential in the ${}^3S_1 + {}^3D_1$ state, and is defined by:

$$v_2(r) = -10.463e^{-x}/x + 105.468e^{-2x}/x - 3187.8e^{-4x}/x + 9924.3e^{-6x}/x, \tag{9.1}$$

where $x = 0.7r$, r is in fm, and v_2 is in MeV.

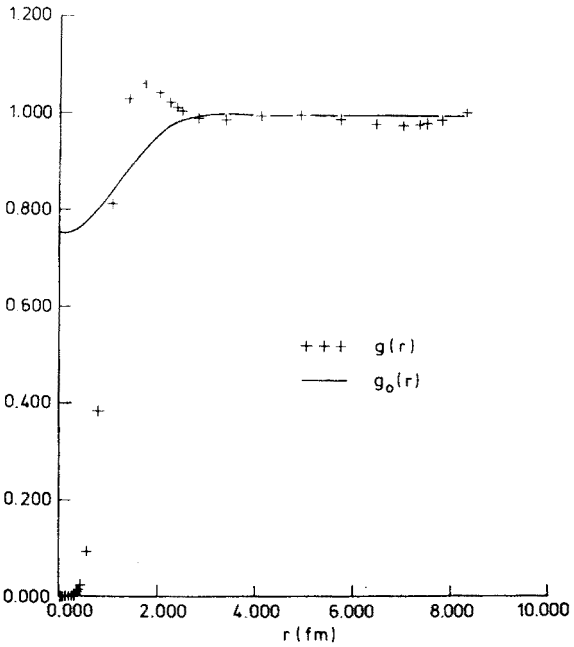

Fig. 9. Functions: g for V_2 potential in LD approximation and g_0 in nuclear matter at $k_F = 1.366\ \mathrm{fm}^{-1}$

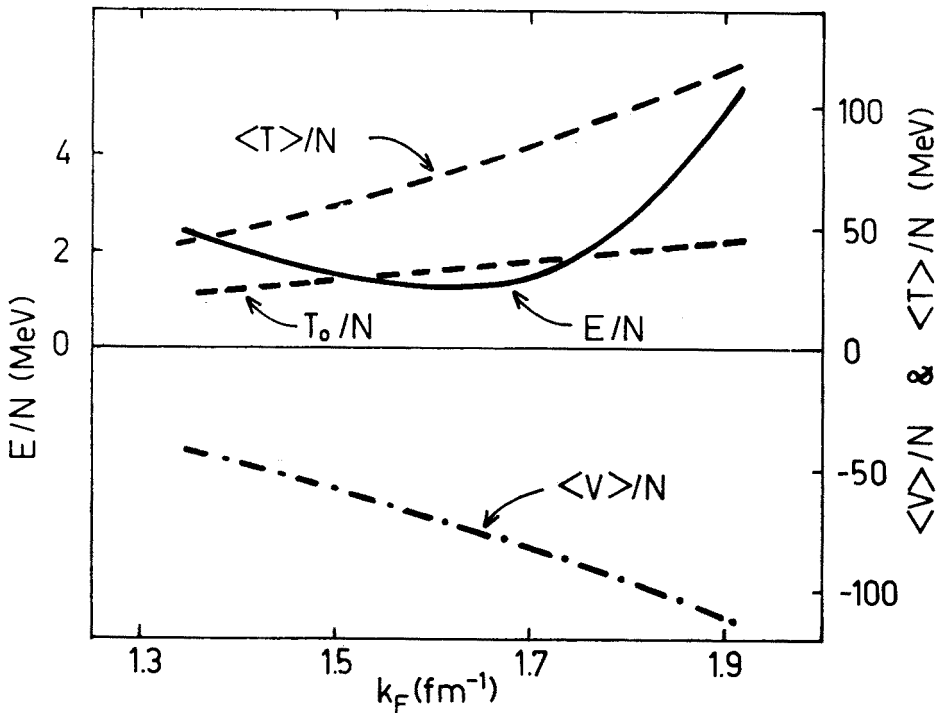

Fig. 10. LD results for $\langle V\rangle$, $\langle T\rangle$, $E_0 = T_0$, and E, for nuclear matter with V_2 potential

Functions g_{LD} and g_0 calculated for $k_F = 1.366\,\mathrm{fm}^{-1}$ are shown in Fig. 9. We used a m-mesh of 5 points here, which is perfectly sufficient for calculating the energy, and the function $g_{LD}(r)$ for small values of r. For large values of r, $u_l(m, r) \cong j_l(mr)$ is a fast oscillating function of m, and a m-mesh of 5 points is not sufficient for an accurate integration, indicated in Eq. (8.15) (with $\hat{\mathscr{F}}_{mM}$ replaced by $\hat{\mathscr{F}}_m$ in our averaged CM momentum approximation). The function g_{LD} should asymptotically approach g_0. The oscillations of g_{LD} around g_0 for $r \gtrsim 5$ fm, visible in Fig. 9, result from our coarse m-mesh. In all our other calculations, we increased the number of points in the m-mesh to 16, and removed the oscillations from the range of r considered.

Results for $\langle V \rangle$, $\langle T \rangle$, $E_0 = T_0$, and E are shown in Fig. 10 as functions of k_F. Our results for E agree with the FHNC results (see, e.g., Fig. 9 of the review by Day [3]).

B. Nuclear matter with pure hard core interaction

Here, we consider the case of pure hard core interaction with radius $c = 0.6$ fm, i.e., the hard core part of the full interaction described in *C*. Strictly speaking, we should call

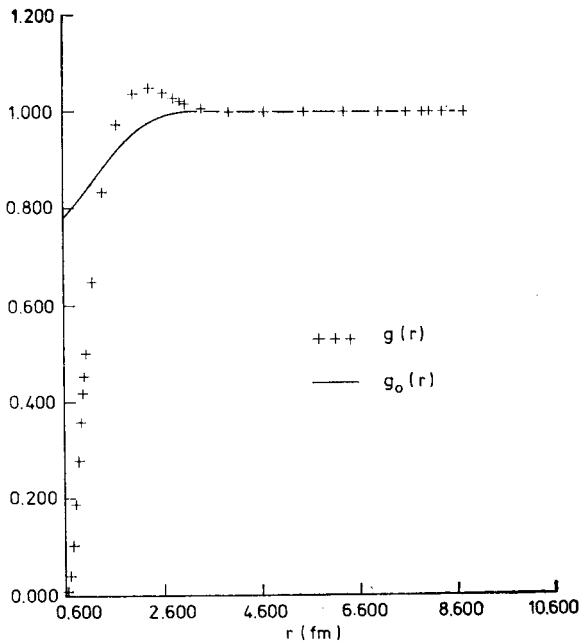

Fig. 11. Functions: g for hard core potential of radius $c = 0.6$ fm in LD approximation and g_0 in nuclear matter at $k_F = 1.366\,\mathrm{fm}^{-1}$

it a hard shell interaction, because of our treatment of the hard core explained after Eq. (8.18).

Functions g_{LD} and g_0 calculated for $k_F = 1.366\,\mathrm{fm}^{-1}$ are shown in Fig. 11. The energy

E which in this case is identical with $\langle T \rangle$ in units of ε_{k_F} is shown in Fig. 12 as function of $x = k_F c$. For comparison, Fig. 12 contains also the result for E of the known expansion in powers of x, which includes terms up to $\sim x^3$ (see, e.g., [6]).

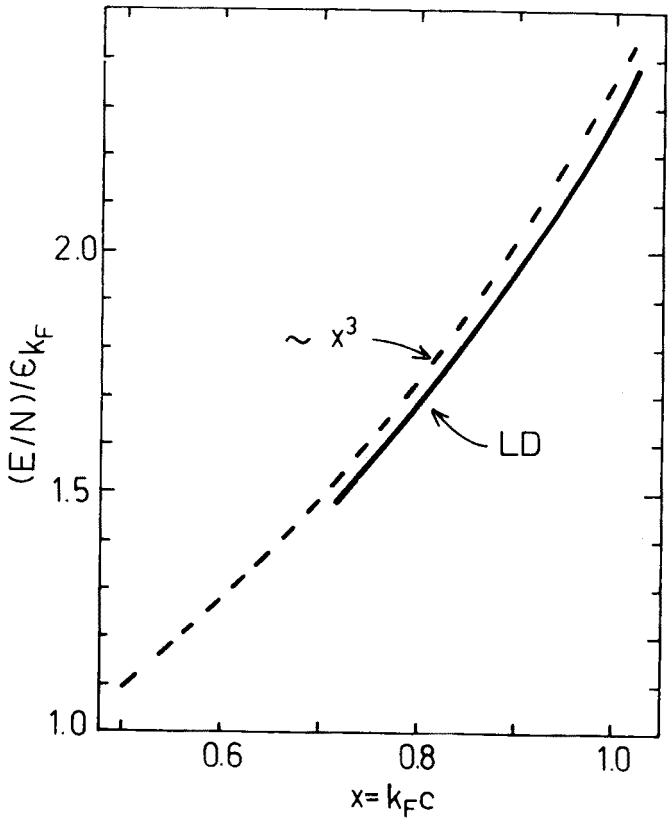

Fig. 12. Energy E of hard core nuclear matter, calculated in the LD and in the x^3 approximations

For the normalization integral I_N, Eq. (2.9), we get $I_N = 0.674$ for $k_F = 1.366\,\mathrm{fm}^{-1}$. The corresponding value of $\kappa = 1 - I_N$ (see Eq. (5.10)) is: $\kappa = 0.326$, which is about twice the value of $\varrho(\frac{4}{3}\pi c^3) = 0.156$.

C. Nuclear matter with OMY6 potential

The index λ, which labels the spin-isospin states, assumes four values denoted in Section 8B as numbers 1, ..., 4 (see Table I). Here, we use an alternative notation: $\lambda = 1 =$ os, $\lambda = 2 =$ et, $\lambda = 3 =$ es, and $\lambda = 4 =$ ot, where "o" stands for odd, "e" for even, "s" for spin-singlet, and "t" for spin-triplet.

The potential OMY6 [12] contains a state independent hard core of radius $c = 0.6$ fm, and its attractive part for $r > c$ is of Serber type, i.e., $v_{os} = v_{ot} = 0$. In the even states,

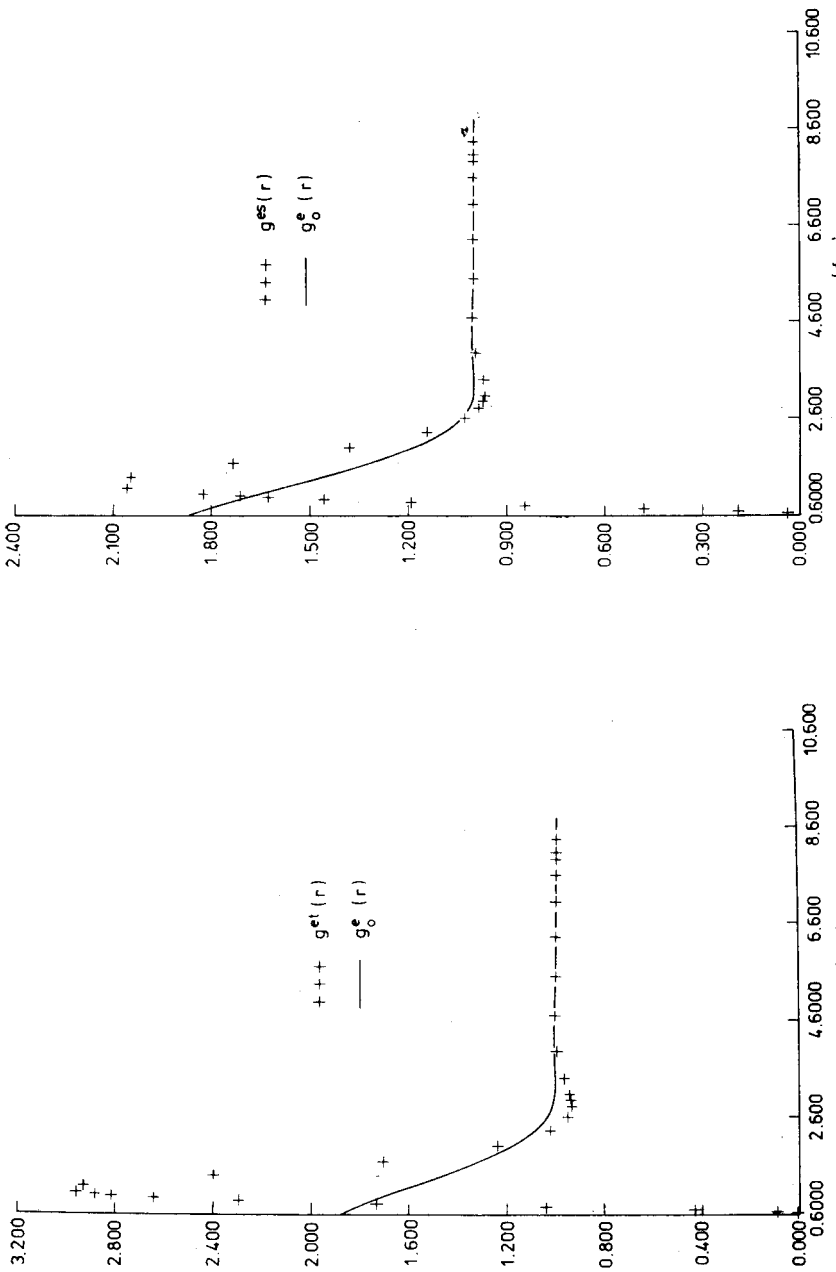

Fig. 13

Fig. 14. Functions: g^{es} for OMY6 potential in LD approximation and g_o^e in nuclear matter at $k_F = 1.366\,\mathrm{fm}^{-1}$

Fig. 13. Functions: g^{et} for OMY6 potential in LD approximation and g_o^e in nuclear matter at $k_F = 1.366\,\mathrm{fm}^{-1}$

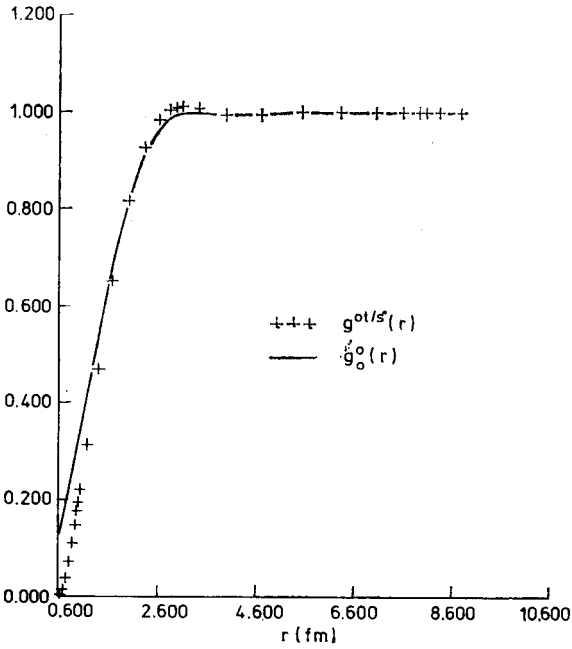

Fig. 15. Functions: $g^{ot/s}$ for OMY6 potential in LD approximation and g_0^o in nuclear matter at $k_F = 1.366\ \text{fm}^{-1}$

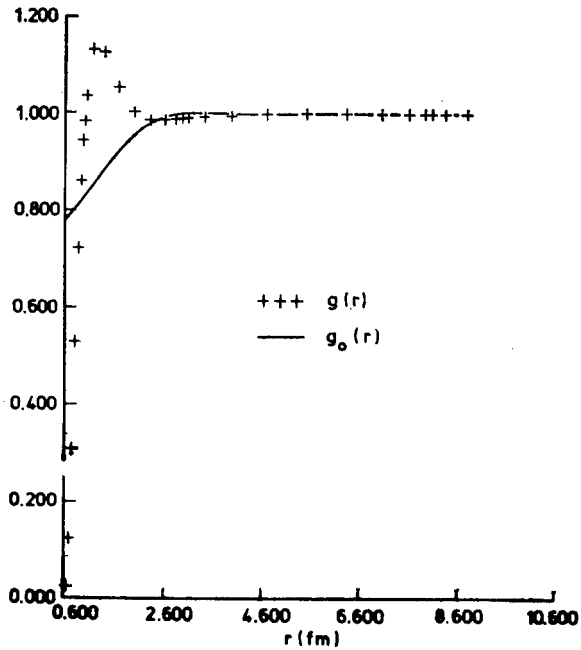

Fig. 16. Functions: g for OMY6 potential in LD approximation and g_0 in nuclear matter at $k_F = 1.366\ \text{fm}^{-1}$

we have:

$$v_{et,s}(r) = v_{t,s}(r) = -V_{t,s} \exp[-\alpha_{t,s}(r-c)], \tag{9.2}$$

where $\alpha_t = 3.6765\,\mathrm{fm}^{-1}$, $\alpha_s = 2.6272\,\mathrm{fm}^{-1}$, $V_t = 947.02$ MeV, and $V_s = 397.31$ MeV.

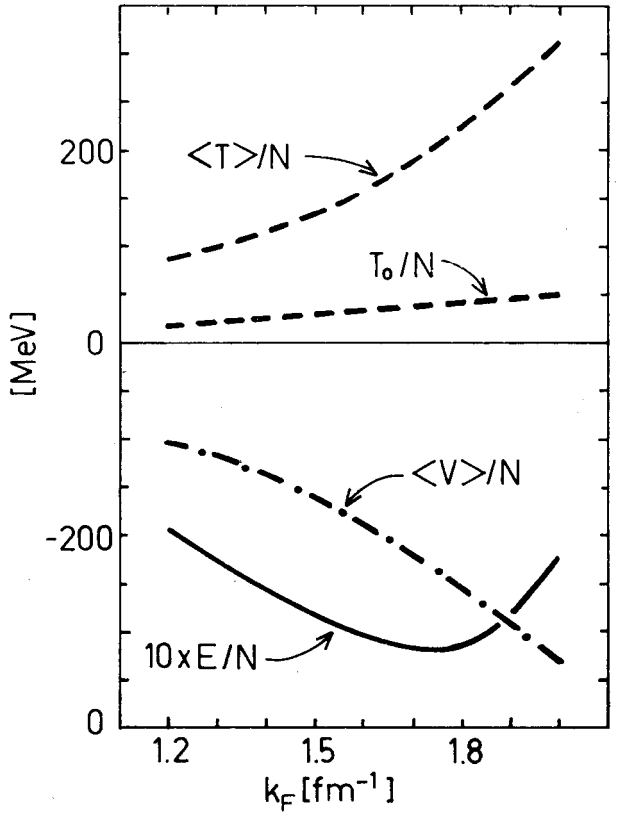

Fig. 17. LD results for $\langle V\rangle$, $\langle T\rangle$, $E_0 = T_0$, and E, for nuclear matter with OMY6 potential

Since in odd l states there is a pure hard core interaction, the wave function in these states $u_l^{\lambda} = s_l$ (λ = os, ot) are the same in spin-singlet and spin-triplet states. Consequently, we have:

$$g^{os} = g^{ot} \equiv g^{ot/s}. \tag{9.3}$$

Obviously, the radial distribution functions $g_0{}^{\lambda}$ of the noninteracting system do not depend on the spin state, and we use the notation:

$$g_0{}^{os}(r) = g_0{}^{ot}(r) \equiv g_0{}^{o}(r) = 1 - l(k_F r)^2, \tag{9.4}$$

$$g_0{}^{et}(r) = g_0{}^{es}(r) \equiv g_0{}^{e}(r) = 1 + l(k_F r)^2. \tag{9.5}$$

All the functions g^{λ}, g calculated in the LD approximation for $k_F = 1.366\,\mathrm{fm}^{-1}$, as well as the corresponding functions $g_0{}^{\lambda}$ and g_0, are shown in Figs 13–16. Results for $\langle V\rangle$ $\langle T\rangle$, $E_0 = T_0$, and E are shown in Fig. 17 as function of k_F.

For the normalization integral I_N, Eq. (2.9), we get $I_N = 0.653$, with the corresponding value of $\kappa = 0.347$.

D. Liquid ^{3}He with LJ 6–12 potential

This is a $\nu = 2$ system. Its empirical equilibrium parameters at zero temperature are: $\varrho = 0.0166$ atoms/Å^3 ($k_F = 0.789$ Å^{-1}), $E/N = -2.53$ °K.

We apply the Lennard–Jones potential (LJ 6–12),

$$v(r) = V_0[(\sigma/r)^{12} - (\sigma/r)^6], \tag{9.6}$$

with $V_0 = 40.88$ °K, and $\sigma = 2.556$ Å (Murphy and Watts [13]).

Functions g_{LD} and g_0, calculated in the LD approximation for $k_F = 0.789$ Å^{-1}, are shown in Fig. 18 which also contains the function g determined experimentally by

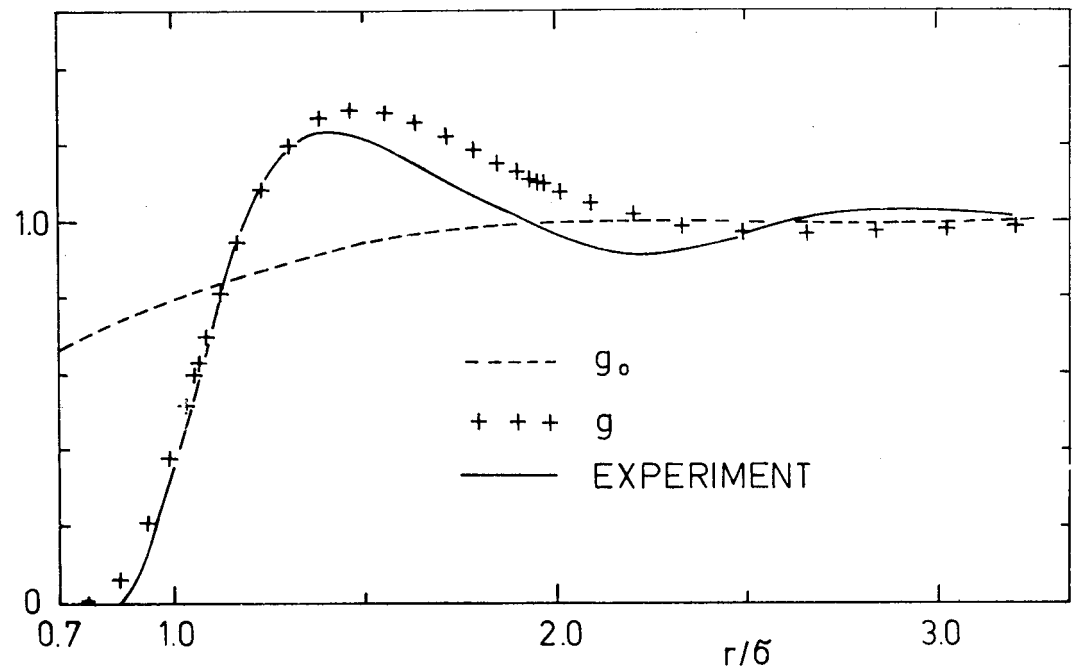

Fig. 18. Functions: g for LJ 6–12 potential in LD approximation and g_0 in liquid ^{3}He at $k_F = 0.789$ Å^{-1}. The experimental curve is taken from Ref. [14]

Achter and Meyer [14]. Results for $\langle V\rangle$, $\langle T\rangle$, $E_0 = T_0$, and E are shown in Fig. 19 as functions of k_F.

For the normalization integral I_N, Eq. (2.9), we get $I_N = 0.260$, with the corresponding value of $\kappa = 0.740$.

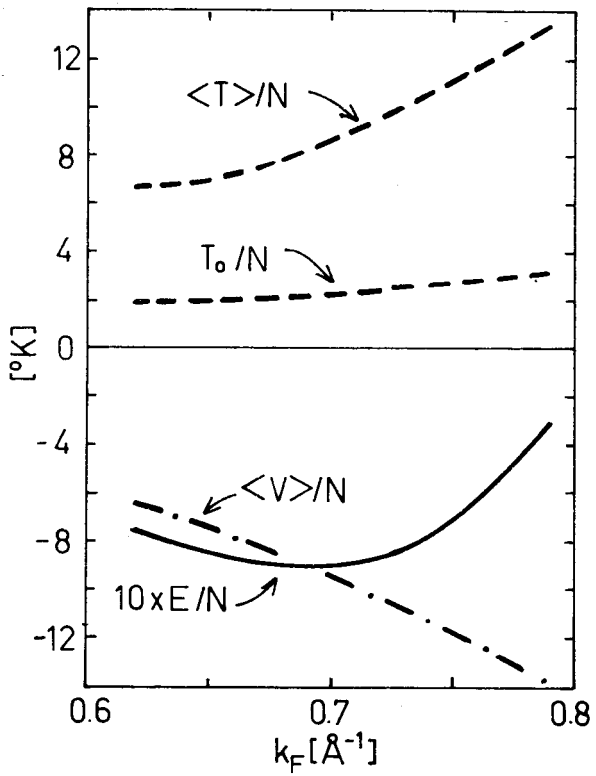

Fig. 19. LD results for $\langle V \rangle$, $\langle T \rangle$, $E_0 = T_0$ and E, for liquid ^{3}He with LJ 6–12 potential

10. The low order Brueckner approximation

In existing calculations of the ground state energy E, the term "low-order-Brueckner" (LOB) approximation is generally used for the procedure in which E is calculated in first order in the self-consistent reaction matrix, and the equation for that matrix contains self-energy insertions into the hole-lines only. This is the so called standard choice of the single nucleon spectrum (here, we use the term "particle" ("hole") when its momentum is bigger (smaller) than k_F, and the term "nucleon" when its momentum is unrestricted).

The LOB approximation was introduced at a time when results indicated that the correction to the total energy due to insertions in particle-states was small. Later results show however that LOB is not a satisfactory approximation. Nevertheless, because of its computational simplicity, it has been and still is used widely in calculations of E. For that reason, we present here the LOB approximation of the radial distribution function.

To simplify the presentation, we disregard spin and isospin in our general derivations, i.e., we put $\nu = 1$, and assume a Wigner type two-body interaction.

A. The LOB1 approximation

We start with writing the result for the radial distribution function in the LOB1 approximation which contains all the LD diagrams plus the LD diagrams with *one* self-

-energy insertion into one of their hole-lines. We have:

$$G_{\mathrm{LOB1}} = G_{\mathrm{LD}} + \Delta_1 G, \tag{10.1}$$

where $\Delta_1 G$ is shown diagrammatically in Fig. 20 which contains all G-diagrams with 3 hole-lines of the self-energy type. Obviously, there are several other G-diagrams with 3 independent hole-lines (some of them are shown in Fig. 5), and this is the reason why the LOB approximation is in itself not a consistent approximation in the sense of the

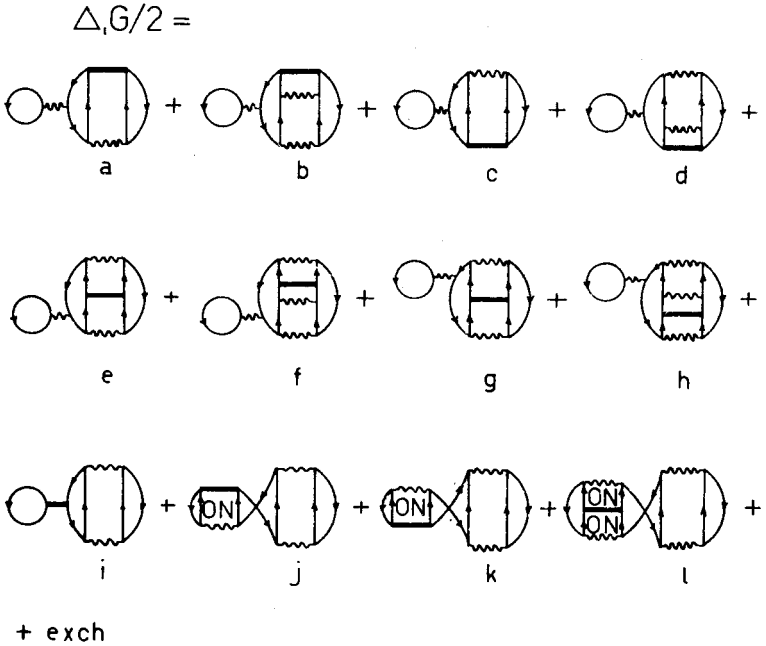

Fig. 20. Diagrams that contribute to $\Delta_1 G$

hole-line expansion. All the other 3 hole-line diagrams should be added for consistency. (This is accomplished by the Faddeev–Bethe equations — see, e.g., [3].)

Diagrams a, c, e, g of Fig. 20 are obtained by simple self-energy insertions into the hole-lines of the corresponding G_{LD}-diagrams. By introducing into diagrams a, c, e, g additional K-interactions between particles, separated from the original K-interaction lines by the self-energy insertions, we obtain diagrams b, d, f, h.

Diagram i of Fig. 20 should also be considered a G-diagram of the hole-self-energy type. Namely, in the calculation of $\langle V \rangle$ (which consists in replacing the heavy lines with broken interaction lines — see the end of Section 3), diagram i contributes to $\langle V \rangle$ a hole--self-energy term. Obviously, together with diagram i, diagrams j, k, l should also be considered as being of the hole-self-energy type.

A common feature of all the diagrams in Fig. 20, which distinguishes them from other three-hole-line diagrams, is that they contain only the on-energy-shell K matrices, i.e., K matrices which satisfy Eq. (4.2). As an illustration let us consider all the contribu-

tions of third order in v to the diagram j, which we denote by $\{\Delta_1 G^{(3)}\}_j/2$. There are two such contributions, and they are shown in Fig. 21. The proof of the last equality in the diagrammatical equation in Fig. 21 is elementary, and practically identical with a similar proof given by Brueckner and Goldman [15]. The symbol "ON" in Fig. 21 means that the energy denominator in the relevant intermediate state is $\varepsilon_{m_1}+\varepsilon_{m_2}-\varepsilon_{k_1}-\varepsilon_{k_2}$. The symbol "ON" in diagrams j, k, l in Fig. 20 has the same meaning.

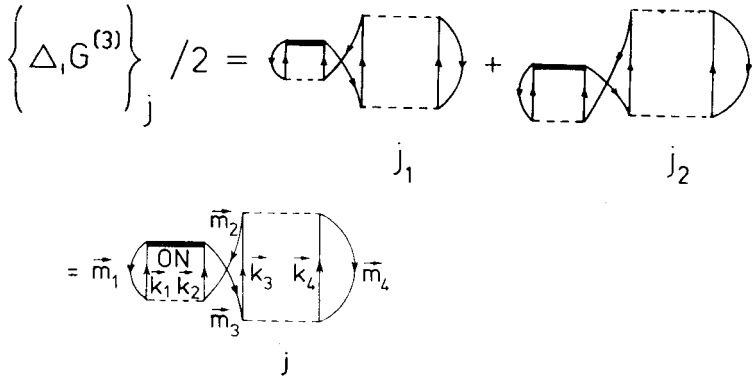

Fig. 21. Diagrams that contribute to the "ON" diagram j of Fig. 20

To obtain the expectation value of V in the LOB1 approximation, $\langle V\rangle_{\mathrm{LOB1}}$, we replace the heavy lines in the G_{LOB1}-diagrams by the broken v-lines, and introduce an extra factor 1/2 (see the end of Section 3). If we take into account the definition of the K matrix, Eq. (4.2), we obtain for $\langle V\rangle_{\mathrm{LOB1}}$ the result (compare the analogous procedure in the LD approximation, Fig. 6):

$$\langle V\rangle_{\mathrm{LOB1}} = \Delta E_{\mathrm{LOB1}} + X_{\mathrm{LOB1}}, \tag{10.2}$$

where ΔE_{LOB1} (the LOB1 approximation of ΔE), and X_{LOB1} are shown in Fig. 22.

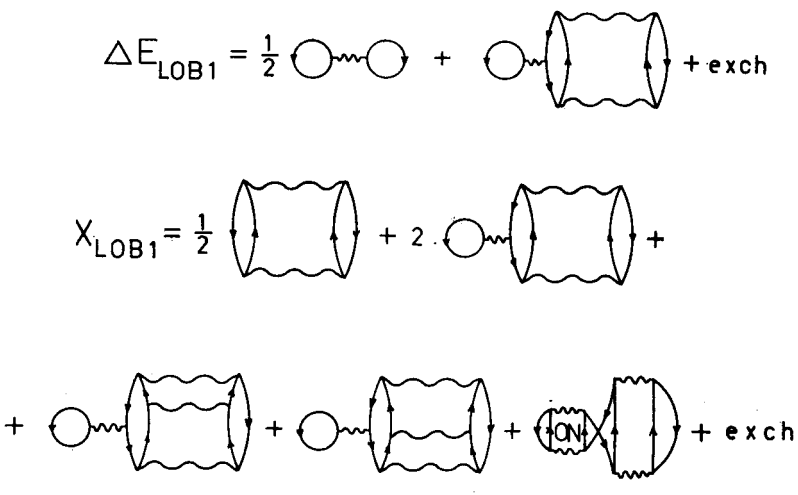

Fig. 22. Diagrams that contribute to ΔE_{LOB1} and X_{LOB1}

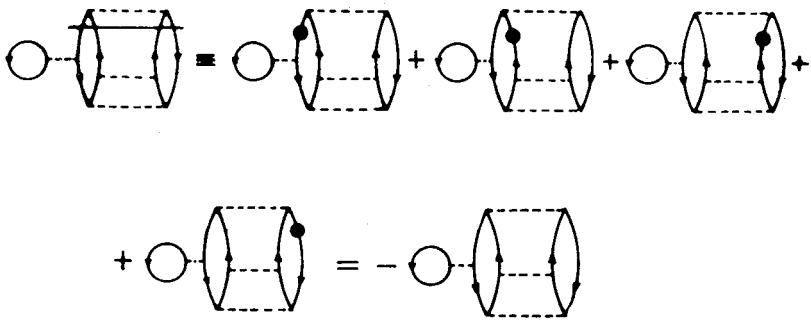

Fig. 23. A class of diagrams that contribute to $\langle \Delta_1 T \rangle^{(4)}$

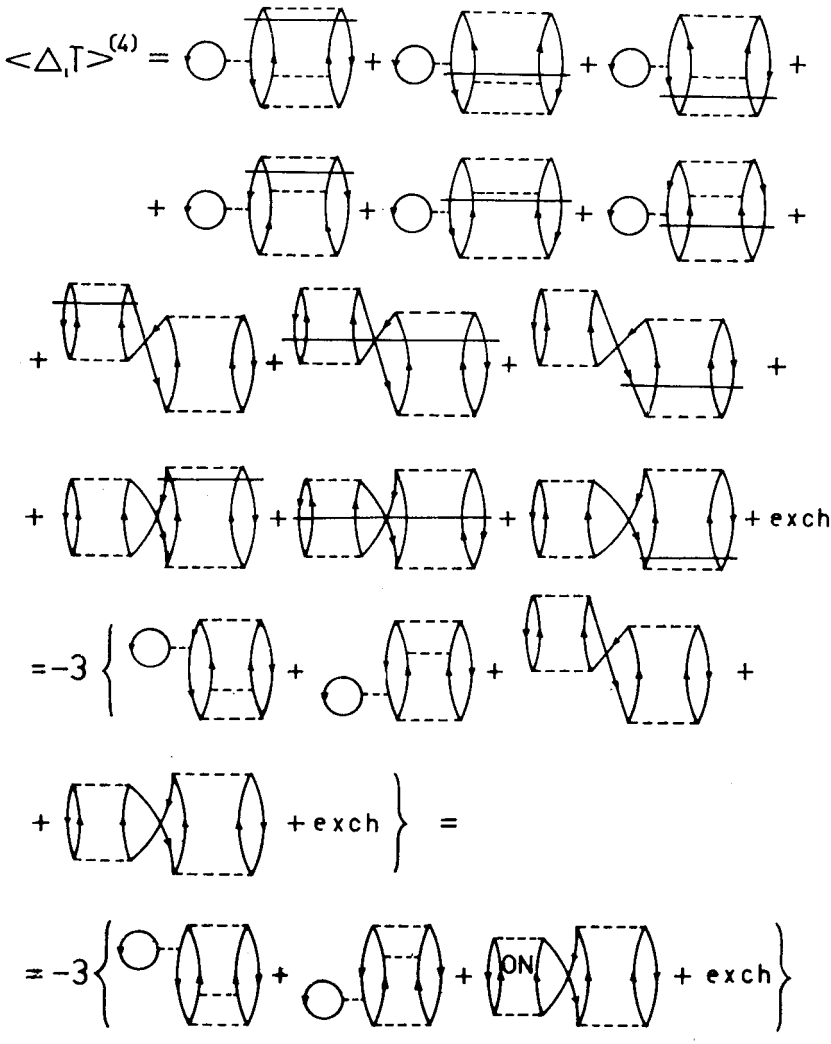

Fig. 24. Diagrams that contribute to $\langle \Delta_1 T \rangle^{(4)}$

To calculate the expectation value of the kinetic energy in the LOB1 approximation $\langle T\rangle_{\mathrm{LOB1}}$, we proceed similarly as in Section 7, and obtain the result:

$$\langle T\rangle_{\mathrm{LOB1}} = \langle T\rangle_{\mathrm{LD}} + \langle \Delta_1 T\rangle, \tag{10.3}$$

where $\langle \Delta_1 T\rangle$ consists of contributions of the 3 hole-line diagrams of the hole-self-energy type. As an illustration let us consider $\langle \Delta_1 T\rangle^{(4)}$, the part of $\langle \Delta_1 T\rangle$ of the fourth order in v. To avoid the necessity of drawing the numerous one-body operator diagrams introduced in Section 7, we introduce a concise notation explained in Fig. 23. The last step in Fig. 23 is accomplished by the same procedure which led to the bottom line in Fig. 7.

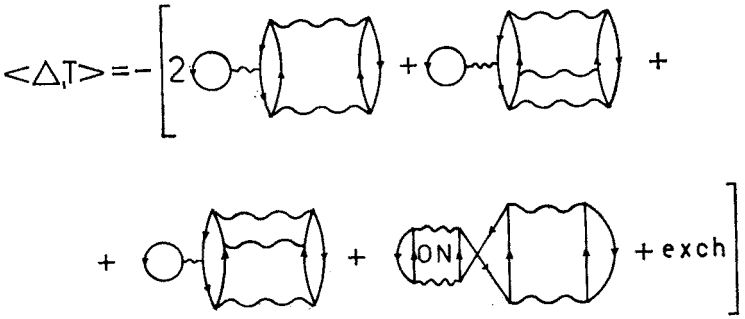

Fig. 25. Diagrams that contribute to $\langle \Delta_1 T\rangle$

The complete expression for $\langle \Delta_1 T\rangle^{(4)}$ is derived diagrammatically in Fig. 24. The last step is the result of the same identity which we used before in Fig. 21. Now, it is easy to see that the result for $\langle \Delta_1 T\rangle^{(4)}$, shown in Fig. 24, is the fourth order (in v) part of the final expression for $\langle \Delta_1 T\rangle$, shown in Fig. 25.

Our result for $\langle \Delta_1 T\rangle$, and our previous result for $\langle T\rangle_{\mathrm{LD}}$ (see Fig. 8), inserted into Eq. (10.3), leads to the result:

$$\langle T\rangle_{\mathrm{LOB1}} = E_0 - X_{\mathrm{LOB1}}. \tag{10.4}$$

Comparing (10.4) with (10.2), we conclude that

$$\langle T\rangle_{\mathrm{LOB1}} + \langle V\rangle_{\mathrm{LOB1}} = E_0 + \Delta E_{\mathrm{LOB1}}, \tag{10.5}$$

i.e., the total energy calculated from the expansion of the radial distribution function, and of the kinetic energy is equal to the expansion of the total energy to the same order. (Compare this result with Eq. (7.4).)

B. The LOB approximation

We are next going to replace the reaction matrix K by a self-consistent reaction matrix $\tilde{K}$ (as in Brueckner theory). In terms of $\tilde{K}$, our expressions for the radial distribution function, potential and kinetic energy will become simpler, and they will contain not only all the LOB1 terms but also numerous other terms.

The $\tilde{K}$ matrix is defined by the equation:

$$\tilde{K}|\phi_{m_1m_2}) = v|\phi_{m_1m_2}) + \sum_{k_1k_2} v|\phi_{k_1k_2}) \left[e_{m_1}+e_{m_2}-\varepsilon_{k_1}-\varepsilon_{k_2}\right]^{-1} (\phi_{k_1k_2}|\tilde{K}|\phi_{m_1m_2}), \quad (10.6)$$

which differs from Eq. (4.2) by the appearance of the self-consistent single-hole energies,

$$e_{m_i} = \varepsilon_{m_i} + V_{m_i}, \quad (10.7)$$

where the single-hole potential

$$V_{m_i} = \sum_{m_j} (\phi_{m_im_j}|\tilde{K}|\phi_{m_im_j} - \phi_{m_jm_i}), \quad (10.8)$$

while particle energies still are kinetic energies ε_k.

We distinguish quantities calculated in the LOB approximation from the corresponding LD quantities by a tilda. For instance, the wave function $\tilde{\psi}$ is defined by

$$\tilde{K}|\phi_{m_1m_2}) = v|\tilde{\psi}_{m_1m_2}), \quad (10.9)$$

and the equation for $\tilde{\psi}$ is:

$$|\tilde{\psi}_{m_1m_2}) - |\phi_{m_1m_2}) \equiv |\tilde{\chi}_{m_1m_2}) = \sum_{k_1k_2} |\phi_{k_1k_2}) \left[e_{m_1}+e_{m_2}-\varepsilon_{k_1}-\varepsilon_{k_2}\right]^{-1} \times (\phi_{k_1k_2}|\tilde{K}|\phi_{m_1m_2}). \quad (10.10)$$

Eq. (4.2) for K, and Eq. (10.6) for $\tilde{K}$ imply the following relation between K and $\tilde{K}$:

$$(\tilde{K}-K)\,|\phi_{m_1m_2}) = \sum_{k_1k_2} K|\phi_{k_1k_2}) \left\{\left[e_{m_1}+e_{m_2}-\varepsilon_{k_1}-\varepsilon_{k_2}\right]^{-1} - \left[\varepsilon_{m_1}+\varepsilon_{m_2}-\varepsilon_{k_1}-\varepsilon_{k_2}\right]^{-1}\right\} (\phi_{k_1k_2}|\tilde{K}|\phi_{m_1m_2}). \quad (10.11)$$

If on the right hand side of (10.11) we keep only terms of lowest order in K, we get

$$\tilde{K}|\phi_{m_1m_2}) \cong K|\phi_{m_1m_2}) - \sum_{k_1k_2m_3} K|\phi_{k_1k_2}) \left[\varepsilon_{m_1}+\varepsilon_{m_2}-\varepsilon_{k_1}-\varepsilon_{k_2}\right]^{-1} \times \left[(\phi_{m_1m_3}|K|\phi_{m_1m_3} - \phi_{m_3m_1}) + (\phi_{m_2m_3}|K|\phi_{m_2m_3} - \phi_{m_3m_2})\right] \times \left[\varepsilon_{m_1}+\varepsilon_{m_2}-\varepsilon_{k_1}-\varepsilon_{k_2}\right]^{-1} (\phi_{k_1k_2}|K|\phi_{m_1m_2}). \quad (10.12)$$

The approximate connection between the matrix elements $(\phi_{p_1p_2}|\tilde{K}|\phi_{m_1m_2})$ and $(\phi_{p_1p_2}|K|\phi_{m_1m_2})$, which follows from Eq. (10.12), is shown diagrammatically in Fig. 26, where a double wavy line denotes $\tilde{K}$.

Notice that the minus sign in Eq. (10.12) is automatically produced by the rule that each hole-line introduces a minus sign. Here, the self-energy insertion into a hole-line introduces an additional hole-line (with the same momentum).

With the help of $\tilde{K}$, we define the LOB approximation of the radial distribution function, G_{LOB}, as is shown in Fig. 27, where a full arrow at a hole-line signals the presence

of single-hole energies e_{m_i} in the propagator (the hole-line is "dressed"). In the *lowest order* in K, the difference between the new LOB and our previous LD propagators is shown in Fig. 28.

If for the $\tilde{K}$ matrices in G_{LOB} we use approximate expression (10.12) (see Fig. 26), and the approximation of Fig. 28 for the LOB hole-lines, and neglect diagrams with more than 3 of these hole lines, we get $G_{\text{LOB}} \cong G_{\text{LOB}1}$. This means that G_{LOB} contains all the 3 hole-line diagrams of the self-energy type. But obviously, it contains much more than that. In particular, it contains multiple self-energy insertions into hole-lines.

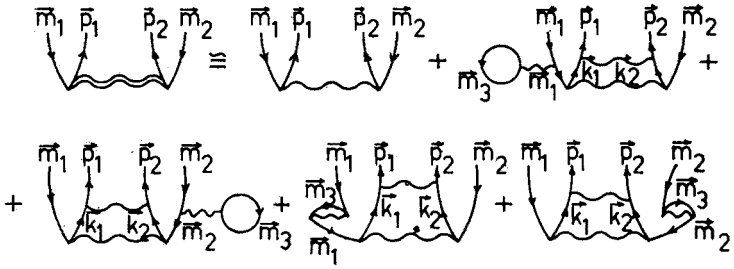

Fig. 26. Diagrammatical representation of the approximate connection between the matrix elements of K and $\tilde{K}$

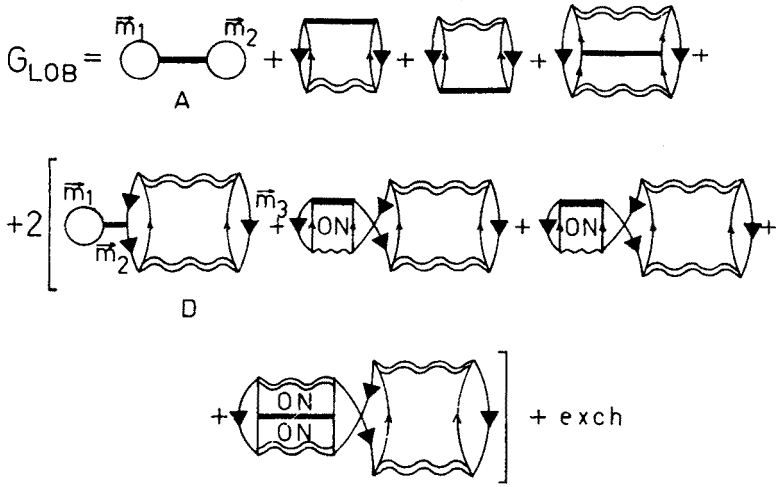

Fig. 27. Diagrams that contribute to G_{LOB}

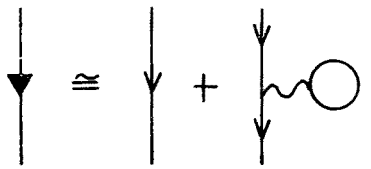

Fig. 28. The approximate connection between bare and dressed hole-lines

The analytical expression for G_{LOB} is easily derived, following the procedure of Section 4:

$$G_{\mathrm{LOB}}(r_1 r_2) = \sum_{m_1 m_2} \tilde{\psi}^*_{m_1 m_2}(r_1 r_2)\,[\tilde{\psi}_{m_1 m_2}(r_1 r_2) - \tilde{\psi}_{m_2 m_1}(r_1 r_2)] \times \{1 - 2\sum_{m_3} (\tilde{\chi}_{m_2 m_3} | \tilde{\chi}_{m_2 m_3} - \tilde{\chi}_{m_3 m_2})\}. \tag{10.13}$$

(Similar expression, however, without the factor in the curly brackets and with an ad hoc normalization factor, was used by Viollier and Walecka [16].)

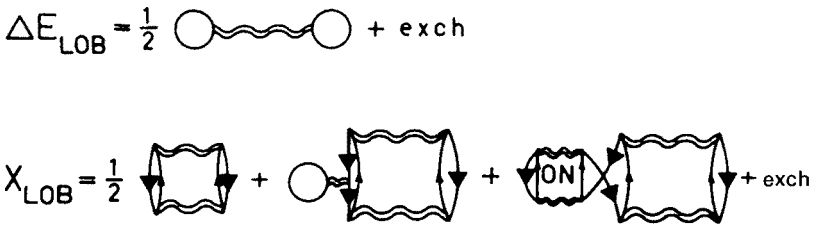

Fig. 29. Diagrams that contribute to ΔE_{LOB} and X_{LOB}

To obtain the expectation value of V in the LOB approximation, $\langle V \rangle_{\mathrm{LOB}}$, we proceed as in the case of the LOB1 approximation with the only difference that now the $\tilde{K}$ matrix equation, Eq. (10.6), must be taken into account. We get:

$$\langle V \rangle_{\mathrm{LOB}} = \Delta E_{\mathrm{LOB}} + X_{\mathrm{LOB}} \tag{10.14}$$

where ΔE_{LOB} (the LOB approximation of ΔE), and X_{LOB} are shown in Fig. 29.

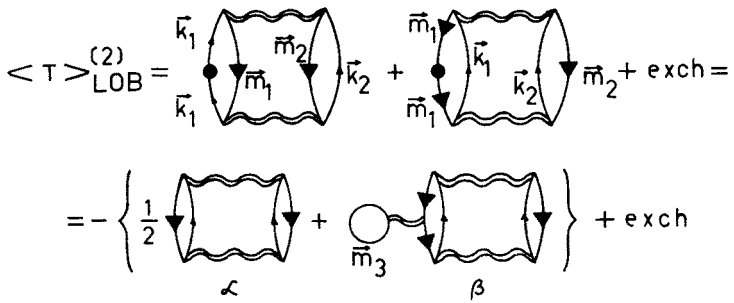

Fig. 30. Diagrams that contribute to $\langle T \rangle^{(2)}_{\mathrm{LOB}}$

We write the expectation value of the kinetic energy in the LOB approximation, $\langle T \rangle_{\mathrm{LOB}}$, in the form:

$$\langle T \rangle_{\mathrm{LOB}} = E_0 + \langle T \rangle^{(2)}_{\mathrm{LOB}} + \langle T \rangle', \tag{10.15}$$

where $\langle T \rangle^{(2)}_{\mathrm{LOB}}$ is shown in Fig. 30. The last step in Fig. 30 was obtained similarly as in the LD approximation (see Eq. (7.2)). We have:

$$\langle T \rangle^{(2)}_{\mathrm{LOB}} = \sum_{k_1 k_2 m_1 m_2} (\phi_{m_1 m_2} | \tilde{K} | \phi_{k_1 k_2})\,[e_{m_1} + e_{m_2} - \varepsilon_{k_1} - \varepsilon_{k_2}]^{-1}$$

$$\times [\varepsilon_{k_1} - \varepsilon_{m_1} - V_{m_1} + V_{m_1}] [e_{m_1} + e_{m_2} - \varepsilon_{k_1} - \varepsilon_{k_2}]^{-1} (\phi_{k_1 k_2} | \tilde{K} | \phi_{m_1 m_2}) + \text{exch}$$

$$= -\tfrac{1}{2} \sum_{k_1 k_2 m_1 m_2} (\phi_{m_1 m_2} | \tilde{K} | \phi_{k_1 k_2}) [e_{m_1} + e_{m_2} - \varepsilon_{k_1} - \varepsilon_{k_2}]^{-1} (\phi_{k_1 k_2} | \tilde{K} | \phi_{m_1 m_2})$$

$$+ \sum_{k_1 k_2 m_1 m_2 m_3} (\phi_{m_1 m_2} | \tilde{K} | \phi_{k_1 k_2}) [e_{m_1} + e_{m_2} - \varepsilon_{k_1} - \varepsilon_{k_2}]^{-1} (\phi_{m_1 m_3} | \tilde{K} | \phi_{m_1 m_3})$$

$$\times [e_{m_1} + e_{m_2} - \varepsilon_{k_1} - \varepsilon_{k_2}]^{-1} (\phi_{k_1 k_2} | \tilde{K} | \phi_{m_1 m_2}) + \text{exch}, \tag{10.16}$$

where we have used definition (10.7) of e_{m_1} and (10.8) of V_{m_1}. Notice the new diagram β in Fig. 30, which appears in the LOB approximation because of the presence of the single-hole potentials in the propagators.

The part $\langle T \rangle'$ of $\langle T \rangle_{\text{LOB}}$ is shown in Fig. 31. Here, we neglect the β diagrams, arising similarly as the β diagram in Fig. 30, as containing four independent hole lines.

A comparison of Figs 30 and 31 with Fig. 29 shows that

$$\langle T \rangle^{(2)}_{\text{LOB}} + \langle T \rangle' = -X_{\text{LOB}} \tag{10.17}$$

and consequently, we have (see Eqs (10.14), (10.15)):

$$\langle T \rangle_{\text{LOB}} + \langle V \rangle_{\text{LOB}} = E_0 + \Delta E_{\text{LOB}}. \tag{10.18}$$

We have thus shown that the total energy calculated in the three-hole-line approximation agrees with the energy calculated from the radial distribution function in the same approximation. Again as in the case of the two-hole-line expansion this is a consistency

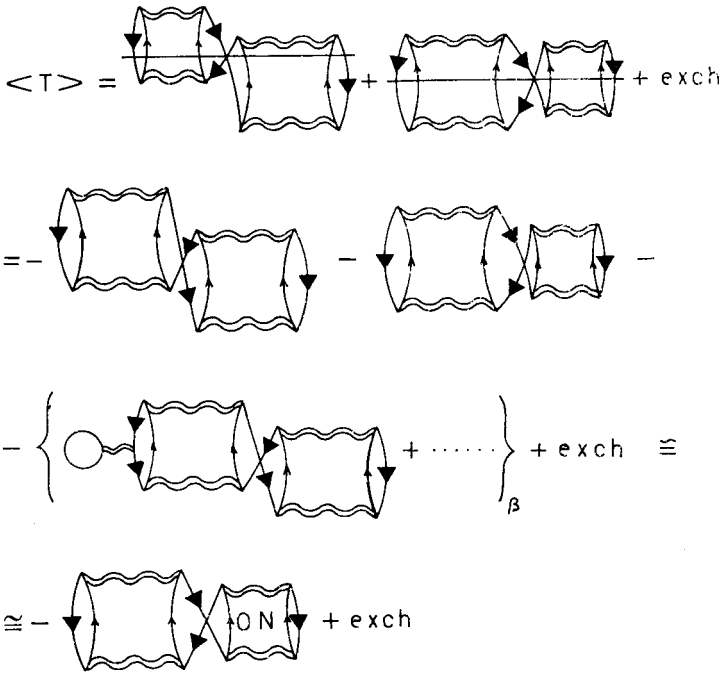

Fig. 31. Diagrams that contribute to $\langle T \rangle'$

check. It is to be noted however that although the potential energy is calculated directly from the radial distribution function, the kinetic energy *is not*. When the kinetic energy is calculated in LOB from a diagram with n hole-lines a diagram with $n+1$ hole lines is generated as shown by the β-diagrams in Figs 30 and 31. This is a consequence of the selfconsistent insertions in hole-lines. (Note that it did not occur in the case of LOB1.) To obtain the selfconsistency result in the case of LOB we therefore had to neglect the β-terms in Fig. 31, which have four-hole-lines.

C. Problems with normalization

Unfortunately G_{LOB} (as well as G_{LOB1}) has a wrong asymptotic behaviour, as may be seen from Eq. (10.13). To see it immediately, let us introduce into Eq. (10.13) the approximation:

$$(\tilde{\chi}_{m_2m_3}|\tilde{\chi}_{m_2m_3}-\tilde{\chi}_{m_3m_2}) \cong N^{-2}\sum_{m_2m_3}(\tilde{\chi}_{m_2m_3}|\tilde{\chi}_{m_2m_3}-\tilde{\chi}_{m_3m_2}) = N^{-1}\tilde{\kappa}. \tag{10.19}$$

Because of the healing property, we have asymptotically (for $r_{12}\to\infty$) $\tilde{\psi}_{m_1m_2}\to\phi_{m_1m_2}$, and consequently Eq. (10.13) leads to:

$$G_{\mathrm{LOB}}(r_1r_2)\to\sum_{m_1m_2}\phi^*_{m_1m_2}(r_1r_2)\,[\phi_{m_1m_2}(r_1r_2)-\phi_{m_2m_1}(r_1r_2)]$$

$$\times\{1-2\tilde{\kappa}\} = G^{(0)}(r_1r_2)\,\{1-2\tilde{\kappa}\}, \tag{10.20}$$

or equivalently:

$$\lim_{r\to\infty} g_{\mathrm{LOB}}(r) = g_0(r)\,\{1-2\tilde{\kappa}\}. \tag{10.21}$$

Since $g_0(r)\to 1$, we see that $1-g_{\mathrm{LOB}}\to 2\tilde{\kappa}$, and consequently the normalization integral I_N, Eq. (2.9), is divergent.

One may easily see that all these difficulties are caused by diagram D in Fig. 27. The disastrous effect of the diagram D on the asymptotic behaviour of the radial distribution function would be cancelled if we introduced the diagram shown in Fig. 32[1]. It appears then that to get consistent results for the radial distribution function it is necessary to introduce together with the hole self-energies simultaneously the particle self-energies.

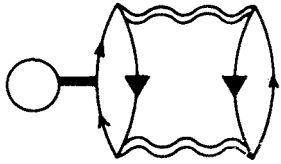

Fig. 32. G-diagram with 3 hole-lines

[1] Compare Fig. 5, where diagrams h, and i give divergent ($\sim N$) contributions to I_N, cancelled however by contributions of diagrams j, and k.

The LOB approximation is a legitimate approximation as far as the calculation of the total energy is concerned, although it is not numerically satisfactory. It is not a consistent three-hole-line expansion however. Only the interaction with a third particle in the hole--line is included but in the particle-line it is not included. As a consequence, we find that the radial distribution function does not have a correct asymptotic behaviour. This comes from the depletion of the hole-states due to the interaction, and that nucleons are not allowed to interact with other nucleons while in particle-states.

11. Summary and conclusions

We have formulated a perturbation theory of the radial distribution function. It is found that the Brueckner technique of summing ladder diagrams of v-interactions can be applied to this problem. The radial distribution function for an interaction with an infinite hard core can therefore be calculated perturbatively.

The summation of different classes of diagrams was considered. The first, the Low--Density (LD) approximation (Section 4) includes all particle–particle ladders but no insertions in particle- or hole-lines. It is therefore a two-hole-line expansion, the hole-lines beeing free (nucleon) propagators carrying kinetic energy only. An important property of the radial distribution function is its normalization. It follows directly from its definition in terms of the normalized wave function of the system. In the LD approximation the radial distribution function is *not* normalized. The error in normalization is equal to the wound integral. The function is on the average too large. This stems from the fact that only particle–particle ladders are included, while the simultaneous depletion of the hole-states is nowhere corrected for in this approximation. One way of satisfying the normalization condition is to define an approximate normalized *wave function* and then calculate the radial distribution function from this. This is shown in Section 5. In Fig. 4 the $2p$–$2h$ states are "free" states, i.e., they have only kinetic energy as in the intermediate states of Fig. 3. In addition to the diagrams of Fig. 3, those shown in Fig. 5 are now generated. The latter diagrams correct for the error in the normalization.

The calculations for nuclear matter and liquid ^{3}He in the LD approximation are preliminary calculations only to serve essentially two purposes. Firstly, we like to illustrate the general methods of applying the formalism. Secondly, a main purpose of our investigation, outlined in the Introduction, is to find the sequential changes in the radial distribution functions by successive inclusion of new types of diagrams. The two-hole-line diagrams with particle ladders are the simplest type diagrams that we can possibly consider. These are the diagrams of the LD approximation. We find the results already interesting at this level. Note, for example, the relative ease with which the state-dependent radial distribution functions are obtained in the case of the OMY6 potential. In a Jastrow approach one has to first define separate correlation functions in different spin-isospin states, which should then be separately varied. In the case of liquid ^{3}He the separate radial distributions for parallel and antiparallel spins can also easily be calculated.

The only experimentally known radial distribution function, among those calculated here, is that of ^{3}He. We find already in our LD approximation a surprising agreement.

In the region $1.3 \lesssim r/\sigma \lesssim 2.5$ we get an overshoot of about 10% and also too large values at very small distances. The overall *positive* error results in a small value of the normalization integral ($I_N = 0.260$) with the corresponding large value of the wound integral ($\kappa = 0.740$). The LD approximation includes only two-body correlations. The only effect of the other particles comes via the exclusion principle. One effect of the presence of other particles would be to prevent the two particles to come close together in certain many-body configurations. The radial distribution function would be suppressed at small distances. The error at $r/\sigma \sim 0.9$ can therefore be understood. The error at larger distances is not as simply explained. However, it is probably closely related to the normalization error and therefore to diagrams in Fig. 5.

In calculations of the energy by Brueckner theory it has been customary to redefine the hole-lines by the inclusion of bubble-insertions. Three-hole-lines, i.e., three-body terms, are therefore actually being introduced. The third line is the bubble. Quite illogically, the resulting theory has however been coined a two-hole-line expansion. There are justifications for this approach. Simply stated: particles in their normally occupied states move in some mean field of the other particles, represented by the bubble-insertions. In excited states this mean field is much less attractive and can be neglected. The ensuing theory contains a one-sided insertion in hole-lines only and is referred to as the LOB approximation (Section 10).

If treated more carefully it is found that the interaction in excited states, in particular at high momenta, cannot be treated as mean field effect. It is rather a *close* collision between three particles. The effect of this can be treated by the three-body equations of Bethe–Faddeev. As a result three-body terms are usually introduced in two steps, the first one being the dressing of the hole-lines, the second the solution of the Bethe–Faddeev equations.

In view of some customary applications of the Brueckner theory, it was considered reasonable to consider the LOB as a next step after the LD approximation. The result was a priori unexpected. While in LD the radial distribution function is not normalized, in LOB it does not even have the correct asymptotic behaviour (Section 10 C). A closer inspection shows that the diagram causing this disaster is the one marked D in Fig. 27. This diagram can be considered as correction to diagram A in the same figure. Nucleon 1 in state $\boldsymbol{m}_1$ does not interact with 2 in its hole state $\boldsymbol{m}_2$ as in A because 2 is partly excited out of $\boldsymbol{m}_1$ due to its correlation with a third nucleon in $\boldsymbol{m}_3$. This correlation is contained in diagram D. In some sense then the wrong asymptotic behaviour in LOB is related to the wrong normalization in LD. Both errors are caused by the depletions of hole-states, that are uncorrected for. In the LOB approximation the error would easily be remedied by including also the diagram in Fig. 32 in the approximation of the radial distribution function. Doing this we would however depart from our original goal, i.e., to consider the LOB approximation. This diagram has an insertion in a particle-line and is only one of the diagrams customarily considered as three-hole-line diagrams.

It is interesting to note that the LOB approximation to the radial distribution function leads to the difficulty mentioned above. In the calculation of the energy there is no similar problem in this approximation. However, it is really just by accidental cancellations of

diagrams that LOB is sometimes an acceptable method in this case. Because of the wrong asymptotic behaviour of the radial distribution function one may in fact question the LOB method as such even as a first order calculation of the energy, the next order being the "three-hole-line diagrams". This is the procedure followed by Day [4].

Given the radial distribution function, the potential energy is directly obtainable (Sections 1 and 2). Our purpose has been to draw as much as possible from the experience gained in energy calculations. We have therefore in both approximations, LD and LOB, in addition to deriving the radial distribution functions derived the kinetic energies to the same respective orders. The total energy obtained in this manner from the two separate calculations of potential and kinetic energy could be shown analytically to be identical to the total energy calculated to the same order. This proof, although it may seem redundant, is of very great value because it allows for a check on the consistent choice of diagrams in each order. The kinetic energy diagrams are one-body diagrams and, except in LD, it is not quite obvious which of these diagrams are the consistent ones. As a matter of fact it was found that some of the kinetic energy diagrams originally picked in LOB were in fact of a higher order and therefore for consistency were neglected (Fig. 31, diagrams β).

We have found that the selection of diagrams used in this paper for the determination of the radial distribution function is not altogether satisfactory. It has led to difficulties with normalization and asymptotic behaviour. Our selection was made in order to stay as close as possible to the selection of diagrams used in Brueckner calculations of the energy. The reason for this was a desire to make a comparison with such calculations at each level of approximation.

However, one may wish to emphasize the comparison with an experimentally determined radial distribution function or liquid structure function. It then appears more important to ascertain that the calculated radial distribution function has the correct properties, e.g., normalization and asymptotic behaviour. This can be achieved by a different selection of diagrams. In the LD approximation such diagrams were already discussed in the text and they include those in Fig. 5. It amounts to considering all $2p-2h$ excitations in the wave function (Fig. 4). In the case of LOB it amounts to adding at least the diagram in Fig. 32 and preferably also other three-hole-line diagrams. We are then actually close to the theory defined above by including the diagrams of Fig. 5 in LD. The only difference is the self-consistent matrix $\tilde{K}$ and the dressed hole-line in LOB.

We shall continue this investigation using the experience gained from the results of this work.

APPENDIX A

Green's functions

In calculating Green's functions $\mathcal{G}_l^{Mm}$, we use Eq. (8.5) for Q, and write Eq. (8.8) in the form ($a = k_F + M/2$):

$$\mathcal{G}_l^{Mm}(rr') = -(\mathcal{M}/2\pi^2)\{\int_{\sqrt{k_F^2 - M^2/4}}^{a} dk k^2 j_l(kr) j_l(kr') Q(M, k)/(k^2 - m^2) + \gamma\}, \qquad \text{(A1)}$$

where

$$\gamma = \int_a^\infty dk k^2 j_l(kr) j_l(kr')/(k^2-m^2) = \mathscr{P}\int_0^\infty dk k^2 j_l(kr)$$

$$j_l(kr')/(k^2-m^2) - \mathscr{P}\int_0^a dk k^2 j_l(kr) j_l(kr')/(k^2-m^2). \tag{A2}$$

In the last step in Eq. (A2), we have artificially introduced integration over the range of k where the function $1/(k^2-m^2)$ is singular, and we have prescribed the way of treating the singularity by taking the principal value of both the integrals. Any other prescription (adding $\pm i\varepsilon$ to k^2-m^2) leads to the same result for γ.

The result of the first integration in (A2) is well known:

$$\mathscr{P}\int_0^\infty dk k^2 j_l(kr) j_l(kr')/(k^2-m^2) = -\tfrac{1}{2}\pi m j_l(mr_<) n_l(mr_>), \tag{A3}$$

where $r_< = \min(r, r')$, and $r_> = \max(r, r')$.

To calculate the second integral in (A2), we write

$$k^2 j_l(kr) j_l(kr')/(k^2-m^2) = [k^2 j_l(kr) j_l(kr')/(k+m)$$

$$-\tfrac{1}{2} m j_l(mr) j_l(mr')]/(k-m) + \tfrac{1}{2} m j_l(mr) j_l(mr')/(k-m). \tag{A4}$$

Now, the first part of expression (A4) is a regular function, and the second part may be integrated immediately.

Our final result is:

$$\mathscr{G}_l^{Mm}(rr') = -(\mathscr{M}/2\pi^2)\{\int_{\sqrt{k_F^2 - M^2/4}}^a dk k^2 j_l(kr) j_l(kr') Q(M, k)/(k^2-m^2)$$

$$-\int_0^a dk[k^2 j_l(kr) j_l(kr')/(k+m) - \tfrac{1}{2} m j_l(mr) j_l(mr')]/(k-m)$$

$$-\tfrac{1}{2}\pi m j_l(mr_<) n_l(mr_>) - \tfrac{1}{2} m \ln(a/m-1) j_l(mr) j_l(mr')\}. \tag{A5}$$

In our calculations, the first two integrals have been computed numerically.

APPENDIX B

Average CM momentum approximation

We found out in our numerical calculations that the double integration over relative and CM momenta, represented by $\hat{\mathscr{S}}_{mM}$, Eq. (8.13), becomes accurate only for such dense m- and M-meshes, for which the number of (m, M) points becomes too big to perform the necessary calculations within a reasonable computer time. Notice that for each (m, M) point, we have to solve integral equations for $u_l^M(m, r)$, Eq. (8.19). On the other hand, the wave functions $u_l^M(m, r)$ depend only weakly on the CM momentum M, and only

these functions introduce the M dependence into the expressions which we have to integrate over m and M.

In this situation, we introduce the average CM momentum approximation [7]. Namely, we introduce for M in $u_l^M(m, r)$ the approximation:

$$M \cong \overline{M}(m) = \sqrt{\langle M^2 \rangle_m}, \tag{B1}$$

where $\langle M^2 \rangle_m$ is the average value of M^2 in the Fermi sea for a fixed value m of the relative momentum,

$$\langle M^2 \rangle_m / k_F^2 = \tfrac{12}{5}(1-\tilde{m})(1+\tfrac{1}{2}\tilde{m}+\tfrac{1}{6}\tilde{m}^2)/(1+\tfrac{1}{2}\tilde{m}). \tag{B2}$$

With approximation (B1), all expressions which we have to integrate over m and M become functions of m only. Consequently, all the $\hat{\mathcal{I}}_{mM}$ integrations are reduced to the $\hat{\mathcal{I}}_m$ integrations, Eq. (8.14).

REFERENCES

[1] E. Feenberg, *Theory of Quantum Fluids*, Academic Press, New York and London 1969.
[2] J. W. Clark, *Prog. Part. Nucl. Phys.*, in press.
[3] B. D. Day, *Rev. Mod. Phys.* **50**, 495 (1978).
[4] B. D. Day, *Recent Progress in Many-Body Theories*, Proceedings, Oaxtepec, Mexico 1981, Springer, Berlin 1981, p. 169.
[5] J. S. Mc Carthy, *Bull. Am. Phys. Soc.* **25**, 737 (1980).
[6] A. L. Fetter, J. D. Walecka, *Quantum Theory of Many-Particle Systems*, Mc Graw-Hill, New York 1971.
[7] D. J. Thouless, *The Quantum Mechanics of Many-Body Systems*, Academic Press, New York 1972.
[8] C. W. Wong, *Phys. Rev. Lett.* **26**, 783 (1971); *Phys. Rev.* **C3**, 1058 (1971).
[9] S. Coon, J. Dąbrowski, *Phys. Rev.* **140**, B287 (1965).
[10] K. A. Brueckner, K. S. Masterson, *Phys. Rev.* **128**, 2267 (1962).
[11] R. V. Reid, *Ann. Phys.* (N.Y.) **50**, 411 (1968).
[12] T. Ohmura, M. Morita, M. Yamada, *Prog. Theor. Phys.* **15**, 222 (1956).
[13] R. D. Murphy, R. O. Watts, *J. Low Temp. Phys.* **2**, 507 (1970).
[14] E. K. Achter, L. Meyer, *Phys. Rev.* **188**, 291 (1969).
[15] K. A. Brueckner, T. G. Goldman, *Phys. Rev.* **117**, 207 (1960).
[16] R. D. Viollier, J. Walecka, *Acta Phys. Pol.* **B8**, 25 (1977).